Chapter 7

Vehicle Stability and Control

Helmut F. Bauer

7.1 INTRODUCTION

In order to analyze properly the performance of rockets and space vehicles, it is necessary to consider the general problem of dynamics and stability of the vehicle under thrust. Since, with the increasing size of space vehicles and their correspondingly larger tank diameters, the liquid propellant frequencies come closer to the control frequency of the vehicle, therefore the influence of the sloshing propellant can no longer be neglected. Also, with this increase in the diameter of the propellant containers, the amount of propellant participating in sloshing and the corresponding liquid forces become rather pronounced and can influence the stability of the vehicle considerably. Since the largest portion of the total weight of the space vehicle is in form of liquid propellant, the problem of interaction of the sloshing propellant with the motion of the space vehicle remains an important consideration throughout the entire powered flight.

The general problem we are concerned with here is the motion of the center of mass, the vehicle attitude, the motion of the propellants in the tanks, and the lateral bending of the vehicle structure under the action of a control system. For the purpose of the following investigations, the rate of mass, the moment of inertia, and acceleration variations were considered small enough to be negligible.[1]

The questions to be answered therefore are how to decrease the influence of propellant sloshing upon the stability of the vehicle by proper container geometry and location, proper choice of the control system and its gain values, and how to obtain the requirements for additional baffles to provide damping of the liquid in the containers. To simplify the analysis, aerodynamic effects and the inertia of the swivel engines, as well as their compliances, are neglected. The control moments will be produced by the swivel engines. The main energy is fed into the system by the feedback loops between the structure of the space vehicle and its control system.

The coordinate system has its origin at the center of mass of the undisturbed vehicle. The accelerated coordinate system is substituted by an inertial system such that the space vehicle is subjected to an equivalent field of acceleration (fig. 7.1). Centrifugal and Coriolis forces, which result from a rota-

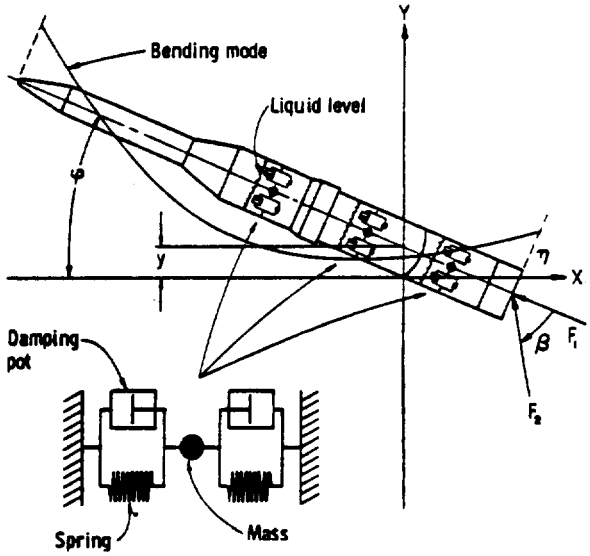

FIGURE 7.1.—Coordinate system of space vehicle.

[1] The equations of motion derived in this chapter are quite simple and are only adequate to illustrate gross effects of the interaction of propellant sloshing, structure, and control.

tion, are considered negligible and the acceleration is in the direction of the trajectory.[2]

7.2 SIMPLIFIED EQUATIONS OF MOTION

In order to outline the problem at hand, we will consider the motion of a flexible body in the plane perpendicular to the trajectory. We define a set of body fixed coordinates, x, y, z, with the origin coinciding with the center of mass. The translatory motion, y, of the vehicle, the rotational motion, ϕ, about the center of mass, as well as the propellant motion, y_n, and the bending vibrations, η_n, are restricted to the x-, y-plane. We follow the conventional method of deriving the equations of motion from Lagrange's equation. It is assumed that the motion of the space vehicle can be described by a superposition of a finite number of preassigned bending mode shapes with a translatory and rotational motion of the vehicle. The elastic mode shapes are introduced as normal modes of vibration of the vehicle structure.

Lagrange's Equation

For the derivation of the equations of motion, we employ Lagrange's equation in the form

$$\frac{d}{dt}\left(\frac{\partial T}{\partial \dot{q}_i}\right)+\frac{\partial D}{\partial \dot{q}_i}+\frac{\partial V}{\partial q_i}=Q_i \qquad (7.1)$$

where T is the kinetic energy of the system, D the dissipation function, and V the potential energy. The generalized forces, Q_i, correspond to those external forces which cannot be derived from a potential. The generalized coordinates, q_i, are independent of each other and specify the configuration of the system at any time, their number representing the number of degrees of freedom of the system. These coordinates are:

y = the lateral translation of the center of mass, or centerline of the undeformed space vehicle

ϕ = the rotational motion of the centerline of the undeformed vehicle about the center of mass, relative to the x-coordinate

y_n = the displacement of the sloshing masses relative to the container wall

η_n = the elastic deflection of the normalized bending mode shape

Kinetic Energy

The kinetic energy is composed of parts arising from motions of the empty structure of the space vehicle and the liquid propellant. The influence of the swivel engines can be neglected. The kinetic energy, T_s, of the empty structure is obtained by summation of the translational and rotational kinetic energy of each segment. The translational velocity, v, resulting from translation, rotation and bending displacements and the angular velocity, ω, are

$$v=\dot{y}-x\dot{\phi}+\sum_{\nu=1}^{\infty}\dot{\eta}_\nu Y_\nu,\quad \omega=\dot{\phi}-\sum_{\nu=1}^{\infty}\dot{\eta}_\nu Y_\nu'$$

where x is the distance of the considered element from the center of mass of the space vehicle, and Y_ν is the normalized bending deflection of the νth lateral bending mode. (The dot indicates differentiation with respect to time, while the prime stands for differentiation with respect to x.) The kinetic energy, T_s, is then

$$T_s=\frac{1}{2}\int m_s'\left(\dot{y}-x\dot{\phi}+\sum_{\nu=1}^{\infty}\dot{\eta}_\nu Y_\nu\right)^2 dx + \frac{1}{2}\int I_s'\left(\dot{\phi}-\sum_{\nu=1}^{\infty}\dot{\eta}_\nu Y_\nu'\right)^2 dx \qquad (7.2)$$

Here, m_s' is the mass of the structure per unit length and I_s' is the mass moment of inertia per unit length about the center of mass of the elemental segment. The integration is performed over the total vehicle length and the bending mode deflection curves, Y_ν, are normalized (to unity) at the swivel point of the engines.

The kinetic energy, T_p, of the liquid propellant can be obtained from an equivalent mechanical model. (See ch. 6.) Such a model describes the linearized liquid motion and may consist of a fixed mass, m_0, and an infinite set of oscillating masses, m_n, which are attached to the propellant container wall by means of springs of stiffness k_n. With this mechanical analogy, the kinetic energy of the propellant can be written as

[2] See refs. 7.1 and 7.2. Other papers on the subject of dynamics of missiles are given in refs. 7.3 through 7.6.

$$T_p=\frac{1}{2}\sum_{\lambda=1}^{l} m_{0\lambda}\left\{\dot{y}-x_{0\lambda}\dot{\phi}+\sum_{\nu=1}^{\infty}\dot{\eta}_\nu Y_\nu(x_{0\lambda})\right\}^2 +\frac{1}{2}\sum_{\lambda=1}^{l} I_{0\lambda}\left\{\dot{\phi}-\sum_{\nu=1}^{\infty}\dot{\eta}_\nu Y'_\nu(x_{0\lambda})\right\}^2 +\frac{1}{2}\sum_{\lambda=1}^{l}\sum_{n=1}^{\infty} m_{\lambda n}\left\{\dot{y}-x_{\lambda n}\dot{\phi}+\sum_{\nu=1}^{\infty}\dot{\eta}_\nu Y_\nu(x_{\lambda n})+\dot{y}_{n\lambda}\right\}^2 \tag{7.3}$$

where l indicates the number of propellant containers, $m_{0\lambda}$ the fixed (nonsloshing) mass in the λth propellant tank, $m_{n\lambda}$ the mass of the nth sloshing mode in the λth container, $x_{0\lambda}$ the distance of the nonsloshing mass in the λth container to the center of mass of the vehicle, and $x_{\lambda n}$ the distance of the nth sloshing mass in the λth container to the center of mass of the vehicle. The value $I_{0\lambda}$ is the moment of inertia of the nonsloshing mass in the λth container about its own center of mass. The displacement of the mass of the nth sloshing mode in the λth container relative to the tank wall is denoted by $y_{n\lambda}$.

Potential Energy

The potential energy is also composed of two main parts; namely, that of the structure and that of the propellant. The potential energy of the structure is again made up of two parts, one of which represents the elastic energy of deformation

$$V_{SE}=\frac{1}{2}\sum_{\nu=1}^{\infty}\eta_\nu^2\left\{\int\frac{M_\nu^2}{EI}\,dx+\int\frac{Q_\nu^2}{A_sG}\,dx\right\}=\frac{1}{2}\sum_{\nu=1}^{\infty}\eta_\nu^2 V_\nu \tag{7.4}$$

and the other represents the work performed in raising the center of mass of the empty vehicle in the gravitational field as the result of rotation. This part becomes, in linearized form

$$V_{sg}=m_s g x_s\frac{\phi^2}{2} \tag{7.5}$$

Equation (7.4) can also be expressed as

$$V_{SE}=\frac{1}{2}\sum_{\nu=1}^{\infty}\omega_\nu^2\eta_\nu^2\left\{\int m'_\nu Y_\nu^2\,dx+\int I'_\nu Y'^2_\nu\,dx\right\}=\frac{1}{2}\sum_{\nu=1}^{\infty}M_{B\nu}\omega_\nu^2\eta_\nu^2 \tag{7.6}$$

Here, M_ν represents the bending moment and Q_ν the shear force acting on an elemental cross section. The flexural stiffness is EI, G is the shear modulus, and A_s represents the shear area of the cross section. The bending frequency of the νth lateral bending mode is ω_ν, and $M_{B\nu}$ represents the generalized mass of the space vehicle. It may be mentioned here that the values $M_{B\nu}$, Y_ν, ω_ν^2 are obtained from a lateral bending analysis.

The potential energy of the propellant is obtained also by using the mechanical analogy and is composed of the energy stored in springs and the raising of the model masses in the gravitational field. The complete expression is:

$$V_p=\frac{1}{2}\sum_{\lambda=1}^{l}\sum_{n=1}^{\infty}k_{\lambda n}y_{n\lambda}^2+\frac{1}{2}g\phi^2\left\{\sum_{\lambda=1}^{l}m_{0\lambda}x_{0\lambda}+\sum_{\lambda=1}^{\infty}\sum_{n=1}^{\infty}m_{n\lambda}x_{n\lambda}\right\}-g\sum_{n=1}^{\infty}\sum_{\lambda=1}^{l}m_{\lambda n}y_{n\lambda}\times\left\{\phi-\sum_{\nu=1}^{\infty}\eta_\nu Y'_\nu(x_{\lambda n})\right\} \tag{7.7}$$

Dissipation Function

The dissipation function of the structure arises from its structural damping, which is considered proportional to the amplitude of the elastic system and in phase with its velocity. This, unfortunately, would lead to complex elements which would complicate the analysis considerably. To avoid this computational complication, a dissipation function is employed which is based on an equivalent linear viscous damping. This is justified as long as the damping forces are small and only of importance in the neighborhood of the bending frequencies.

The dissipation function of the structure is therefore given by

$$D_s=\frac{1}{2}\sum_{\nu=1}^{\infty}\omega_\nu M_{B\nu}g_\nu\dot{\eta}_\nu^2 \tag{7.8}$$

where g_ν is the dimensionless structural damping coefficient of the νth lateral bending vibration mode, and ranges in the neighborhood of $0.001\leq g_\nu\leq 0.05$.

The dissipation function of the liquid propellant arises from the equivalent linear viscous damping as it was introduced by linear dashpots

in the mechanical model. (See ch. 6.) This takes the form, with $c_{\lambda n}=2\zeta_{n\lambda}\omega_{n\lambda}m_{n\lambda}$

$$D_p=\frac{1}{2}\sum_{\lambda=1}^{l}\sum_{n=1}^{\infty}c_{n\lambda}\dot{y}_{\lambda n}^2=\sum_{\lambda=1}^{l}\sum_{n=1}^{\infty}\zeta_{n\lambda}\omega_{n\lambda}m_{n\lambda}\dot{y}_{\lambda n}^2 \quad (7.9)$$

where $\zeta_{n\lambda}$ is the damping factor and $\omega_{n\lambda}$ is the circular natural frequency of the nth sloshing mode in the λth container.

Generalized Mass

The equations of motion are to be obtained by performing differentiations for each generalized coordinate in the Lagrange equation, where the following relations have to be observed.

The total mass, m, of the vehicle is given by (engine mass neglected)

$$m=\int m_s'\,dx+\sum_{\lambda=1}^{l}m_{0\lambda}+\sum_{\lambda=1}^{l}\sum_{n=1}^{\infty}m_{n\lambda} \quad (7.10)$$

The origin of the coordinate system is at the equilibrium position of the center of mass of the total space vehicle, which is expressed by the equation

$$\int m_s'x\,dx+\sum_{\lambda=1}^{l}m_{0\lambda}x_{0\lambda}+\sum_{\lambda=1}^{l}\sum_{n=1}^{\infty}m_{n\lambda}x_{n\lambda}=0 \quad (7.11)$$

Furthermore, the linear momentum for the normal modes of vibration is conserved and expressed by

$$\int m_s'Y_\nu\,dx+\sum_{\lambda=1}^{l}m_{0\lambda}Y_\nu(x_{0\lambda})+\sum_{\lambda=1}^{l}\sum_{n=1}^{\infty}m_{n\lambda}Y_\nu(x_{n\lambda})=0 \quad (7.12)$$

where the integrations are to be performed along the total vehicle length.

Generalized Thrust Forces

Before proceeding to the derivation of the equations of motion, the generalized forces that cannot be represented from a potential are derived. These are obtained by calculating the virtual work done by the external forces through virtual increments, δq_i, of the generalized coordinates, q_i. Thus,

$$\delta W=\sum Q_i\delta q_i$$

where W is the work and Q_i are the generalized forces. Since we neglect aerodynamic forces and propellant flow forces in the pipelines, the only force we shall be concerned with will be that of the vehicle thrust, F. If only a part, F_2, of the thrust $F=F_1+F_2$ is employed for control purposes, that is, if only this part of the total thrust can be gimbaled, while the remainder, F_1, of the thrust is stationary, then the derivation of the generalized forces with respect to the thrust is as follows.

The generalized force of the lateral translation resulting from the thrust vector of the vehicle is given by the thrust component in the y-direction. The virtual work is (see fig. 7.2)

$$\delta W_y=F\left\{\phi-\sum_{\nu=1}^{\infty}\eta_\nu Y_\nu'(x_E)\right\}\delta y+F_2\beta\delta y$$

from which the generalized force, Q_y, is obtained as

$$Q_y=F\left\{\phi-\sum_{\nu=1}^{\infty}\eta_\nu Y_\nu'(x_E)\right\}+F_2\beta \quad (7.13)$$

where β is the engine deflection as measured from the centerline of the vehicle. The generalized force of rotation is presented by the moment of the thrust force about the center of mass of the vehicle, and with

$$\delta W_\phi=F\left\{x_E\sum_{\nu=1}^{\infty}\eta_\nu Y_\nu'(x_E)-\sum_{\nu=1}^{\infty}\eta_\nu Y_\nu(x_E)\right\}\delta\phi-F_2x_E\beta\delta\phi$$

gives the expression

$$Q_\phi=F\left\{x_E\sum_{\nu=1}^{\infty}\eta_\nu Y_\nu'(x_E)-\sum_{\nu=1}^{\infty}\eta_\nu Y_\nu(x_E)\right\}-F_2x_E\beta \quad (7.14)$$

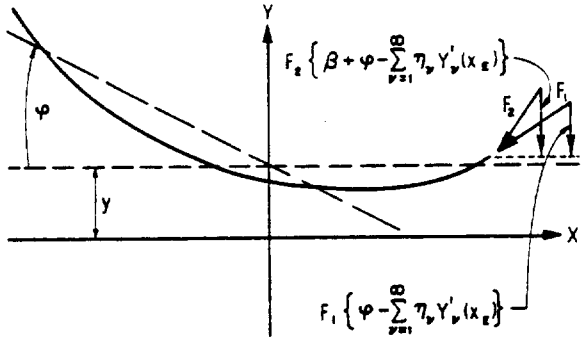

FIGURE 7.2.—Generalized forces resulting from thrust.

Finally, the generalized force of the thrust with respect to the generalized coordinates arising from the lateral bending of the space vehicle are obtained in a similar way by observing that the thrust force is always perpendicular to the lateral bending motion and that the virtual work through a virtual displacement of the generalized coordinate, η_ν, is

$$\delta W_{\eta_\nu} = F_2 \beta Y_\nu(x_E)\delta\eta_\nu$$

The generalized force is therefore

$$Q_{\eta_\nu} = F_2 \beta Y_\nu(x_E) \tag{7.15}$$

The generalized forces of the thrust with respect to the sloshing displacement are zero; i.e., $Q_{\psi_n}=0$.

Translational Equation of Motion

The equation of motion for translation, y, of the vehicle is obtained from equation (7.1), with equations (7.2) and (7.3), by employing the results equations (7.10) through (7.13), thus

$$m\ddot{y}+\sum_{\lambda=1}^{l}\sum_{n=1}^{\infty} m_{n\lambda}\ddot{y}_{n\lambda} = F\phi + F_2\beta - F\sum_{\nu=1}^{\infty}\eta_\nu Y'_\nu(x_E) \tag{7.16}$$

Pitching Equation of Motion

The equation of motion of the vehicle in pitching, ϕ, is obtained from equation (7.1) with $q_i=\phi$, and employing equations (7.2) through (7.14), thus

$$I\ddot{\phi}-\sum_{n=1}^{\infty}\sum_{\lambda=1}^{l} m_{n\lambda}x_{n\lambda}\ddot{y}_{n\lambda} - g\sum_{n=1}^{\infty}\sum_{\lambda=1}^{l} m_{n\lambda}y_{n\lambda} + F_2 x_E\beta = F\left\{x_E\sum_{\nu=1}^{\infty}\eta_\nu Y'_\nu(x_E) - \sum_{\nu=1}^{\infty}\eta_\nu Y_\nu(x_E)\right\} \tag{7.17}$$

where the effective moment of inertia of the space vehicle is given by

$$I = mk^2 = \int m'_s x^2 dx + \int I'_s dx + \sum_{\lambda=1}^{l} m_{0\lambda}x_{0\lambda}^2 + \sum_{\lambda=1}^{l} I_{0\lambda} + \sum_{n=1}^{\infty}\sum_{\lambda=1}^{l} m_{n\lambda}x_{n\lambda}^2 \tag{7.18}$$

and the equation for the conservation of the angular moment has been observed as

$$\int m'_s x Y_\nu(x)dx + \int I'_s Y'_\nu(x)dx + \sum_{\lambda=1}^{l} m_{0\lambda}x_{0\lambda}Y_\nu(x_{0\lambda}) + \sum_{\lambda=1}^{l} I_{0\lambda}Y'_\nu(x_{0\lambda}) + \sum_{n=1}^{\infty}\sum_{\lambda=1}^{l} m_{n\lambda}x_{n\lambda}Y_\nu(x_{n\lambda}) = 0 \tag{7.19}$$

The value x_E is the distance of the swivel point of the engines from the origin and k is the radius of gyration of the vehicle. The right-hand side of equation (7.17) represents the generalized force of the thrust with respect to lateral bending. The values $Y_\nu(x_E)$ and $Y'_\nu(x_E)$ are the lateral displacement and slope of the νth bending mode at the location of the swivel point, respectively.

Propellant Equation of Motion

The equation of motion of the moving propellant in the containers of the vehicle is based on the mechanical model and is obtained by applying the Lagrange equation to the generalized coordinate $y_{n\lambda}$ observing that the generalized force, $Q_{\psi_{n\lambda}}$, vanishes. This yields the equation of the modal sloshing mass (refs. 7.7 and 7.8)

$$\ddot{y}_{n\lambda}+2\zeta_{n\lambda}\omega_{n\lambda}\dot{y}_{n\lambda}+\omega_{n\lambda}^2 y_{n\lambda} = -\left\{\ddot{y}-x_{n\lambda}\ddot{\phi}+\sum_{\nu=1}^{\infty}\ddot{\eta}_\nu Y_\nu(x_{n\lambda})\right\} + g\left\{\phi-\sum_{\nu=1}^{\infty}\eta_\nu Y'_\nu(x_{n\lambda})\right\}$$
$$\lambda=1, 2, \ldots l;\ n=1, 2 \ldots \tag{7.20}$$

The subscript n indicates the number of the propellant mode under consideration, while λ indicates the container number. $\zeta_{n\lambda}$ is the damping factor of the propellant and $\omega_{n\lambda}$ is the undamped circular natural frequency. $Y_\nu(x_{n\lambda})$ and $Y'_\nu(x_{n\lambda})$ are displacement and slope, respectively, of the νth lateral bending mode at the location of the nth sloshing mass in the λth container.

Lateral Bending Equation of Motion

As vehicles increase in size, the lateral fundamental bending frequency approaches more and more closely to the control frequency and

the lower natural frequencies of the propellant. This indicates that in many cases the bending vibrations of the vehicle cannot be neglected in a dynamic analysis of the vehicle that also includes propellant sloshing and the control system. (See ch. 9.)

The equation of motion of the νth bending mode is obtained from equation (7.1) together with equations (7.2) through (7.7) and by noting the results of equations (7.12), (7.19), and the orthogonality relations between normal modes, as expressed by

$$\int m'_s Y_\nu(x) Y_\mu(x)dx+\int I'_s Y'_\nu(x)Y'_\mu(x)dx$$
$$+\sum_{\lambda=1}^{l} m_{0\lambda}Y_\nu(x_{0\lambda})Y_\mu(x_{0\lambda})+\sum_{\lambda=1}^{l} I_{0\lambda}Y'_\nu(x_{0\lambda})Y'_\mu(x_{0\lambda})$$
$$+\sum_{n=1}^{\infty}\sum_{\lambda=1}^{l} m_{n\lambda}Y_\nu(x_{n\lambda})Y_\mu(x_{n\lambda})=0 \quad (7.21)$$

thus

$$\ddot{\eta}_\nu+g_\nu\omega_\nu\dot{\eta}_\nu+\omega_\nu^2\eta_\nu=\frac{F_2}{M_{B\nu}}Y_\nu(x_E)\beta$$
$$-\frac{g}{M_{B\nu}}\sum_{n=1}^{\infty}\sum_{\lambda=1}^{l} m_{n\lambda}y_{n\lambda}Y'_\nu(x_{n\lambda})$$
$$-\frac{1}{M_{B\nu}}\sum_{n=1}^{\infty}\sum_{\lambda=1}^{l} m_{n\lambda}\ddot{y}_{n\lambda}Y_\nu(x_{n\lambda}) \quad (7.22)$$

Here, ω_ν represents the natural circular frequency of the νth lateral bending mode and g_ν is the corresponding structural damping. The generalized mass of the νth lateral bending mode, $M_{B\nu}$, is given by the expression

$$M_{B\nu}=\int m'_s Y_\nu^2(x)dx+\int I'_s Y'^2_\nu(x)dx$$
$$+\sum_{\lambda=1}^{l} m_{0\lambda}Y_\nu^2(x_{0\lambda})+\sum_{\lambda=1}^{l} I_{0\lambda}Y'^2_\nu(x_{0\lambda})$$
$$+\sum_{n=1}^{\infty}\sum_{\lambda=1}^{l} m_{n\lambda}Y_\nu^2(x_{n\lambda}) \quad (7.23)$$

The values $Y_\nu(x_{0\lambda})$ and $Y'_\nu(x_{0\lambda})$ represent nothing but the displacement and slope of the νth lateral bending mode at the location of the nonsloshing mass in the λth propellant tank.

Control System Equation of Motion

Actually, the control equation cannot be expressed as a linear equation; however, translational and rotational motions of the space vehicle usually occur at sufficiently small frequencies so that the control elements can be considered as essentially linear. Nonlinearities usually occur at higher frequencies in the form of saturation of amplifiers, limited output of velocities, and so forth. The control equation is written, therefore, in the form

$$f_1(\beta)=f_2(\phi_i, A_i)$$

where the operators f_1 and f_2 are functions that depend on the character of the system. A_i is the indicated acceleration, as measured by an accelerometer normal to the longitudinal axis of the vehicle. In linear form one can express this as

$$\sum_\nu p_\nu\frac{d^\nu\beta}{dt^\nu}=\sum_j a_j\frac{d^j\phi_i}{dt^j}+\sum_\kappa g_{\kappa+2}\frac{d^\kappa A_i}{dt^\kappa} \quad (7.24)$$

Here, the p_ν are the so-called phase-lag coefficients, and ϕ_i is the indicated angular deviation from the trajectory as indicated by the gyroscope

$$\phi_i=\phi-\sum_{\nu=1}^{\infty}\eta_\nu Y'_\nu(x_G) \quad (7.25)$$

where $Y'_\nu(x_G)$ is the derivative of the νth lateral bending mode at the location of the gyroscope. If the fundamental lateral bending frequency is well above the control and propellant sloshing frequencies, of which the corresponding sloshing masses create pronounced dynamic effects, the flexibility of the space vehicle can be neglected and the control equation can be written in the simplified form ($\nu=0$; $j=1, 2$, $\kappa=0$, and $p_0=1$)

$$\beta=a_0\phi+a_1\dot{\phi}+g_2A_i \quad (7.26)$$

Here, time derivatives in β, which produce increasing phase lags with increasing frequency, have been neglected. In order to include the effect of the flexible structure, the phase-lag coefficients are of importance and have to be considered. A still simplified control equation for these cases would be of the form

$$p_2\ddot{\beta}+p_1\dot{\beta}+\beta=a_0\phi_i+a_1\dot{\phi}_i+g_2A_i \quad (7.27)$$

which only approximately describes the complexity of an actual control system. By proper choice of the phase-lag coefficients, p_1 and p_2, and by proper choices of the attitude value, a_0, and the rate value, a_1, the control system can be approximated. A simple system is preferred for this type of analysis in order to keep the analysis and the interpretation lucid, and still render good results. If no accelerometer is employed for control purposes, the gain value, g_2, vanishes. This term, g_2, is a measure of the strength with which the control accelerometer influences the control of the space vehicle.

The attitude gyroscope is a free gyroscope that measures the position of the vehicle, the main function of the gyroscope being to maintain a space-fixed angular reference. Since we restrict our motion to one plane only (pitching), we consider only the appropriate gyroscope of the stable platform. The essential property of a gyroscope is used, which represents an angular velocity about an orthogonal axis (output axis), if a torque is applied about an input axis. If the platform on which the gyroscope is mounted is perfectly balanced and the bearings are frictionless, no torque will be experienced by the platform, thus maintaining its orientation regardless of the motion of the space vehicle (ref. 7.9). The pickoffs of the gyroscope must be very light in weight and should not introduce any torques; this can be achieved by various forms of capacitive, inductive, or optical pickoffs. Because of unbalances and friction, which cannot be eliminated completely, a disturbance torque is exerted on the stable platform; a servosystem counteracts this disturbing torque and produces essentially a torque-free system. For the purposes of this chapter, we consider a properly designed gyroscope which exhibits a transfer function of unity for a very large bandpass. This means that the indicated attitude angle will be the same as the input angle and is described by equation (7.25).

Accelerometer Equation of Motion

A vehicle moving in the pitch plane possesses two rigid body degrees of freedom, one translational degree of freedom in the y-direction and one rotational degree of freedom denoted by ϕ. While the gyroscope detects rotational motion, the accelerometer is required to provide a reference for translational motion. An accelerometer and a gyroscope are therefore capable of supplying information about the motion of a rigid space vehicle in the pitch plane (x, y plane). In addition to the gyroscope, an accelerometer provided for control purposes can, by proper choice of the gain value and its vibrational characteristics, also diminish loads and reduce engine angle requirements of the swivel engines. Mounting an accelerometer to the structure of the vehicle such that its sensitive direction is perpendicular to the longitudinal axis of the vehicle, this instrument is then capable of sensing the accelerations due to translation, pitching, and bending motions.

The equation of motion of an accelerometer (shown schematically in fig. 7.3) can be obtained from Lagrange's equation. The kinetic energy is given by

$$T=\frac{m_a}{2}\left\{\dot{y}-x_a\dot{\phi}+\dot{y}_a+\sum_{r=1}^{\infty}\dot{\eta}_r Y_r(x_a)\right\}^2$$

where y_a is the relative deflection of the accelerometer mass, m_a, with respect to the space vehicle, and $(-x_a)$ is the location of the accelerometer measured from the mass center of the vehicle. The dissipation function corresponding to linear damping can be represented by

$$D=\frac{c_a}{2}\dot{y}_a^2$$

where c_a is the damping coefficient. The potential energy is

$$V=\frac{k_a}{2}y_a^2-m_a g y_a\left\{\phi-\sum_{r=1}^{\infty}\eta_r Y_r'(x_a)\right\}$$

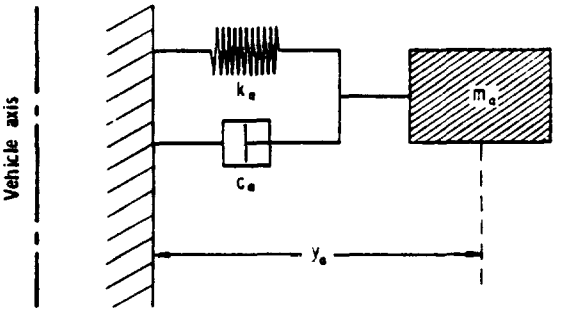

FIGURE 7.3.—Schematic of accelerometer.

The first term is the energy stored in the spring, while the second term is the potential energy decrease resulting from the change of location of the mass, m_a, in the equivalent acceleration field, g. With these results, the equation of motion of the accelerometer is obtained by applying Lagrange's equation to yield

$$m_a\left\{\ddot{y}-x_a\ddot{\phi}+\ddot{y}_a+\sum_{\nu=1}^{\infty}\ddot{\eta}_\nu Y_\nu(x_a)\right\}+c_a\dot{y}_a+k_a y_a$$
$$=m_a g\left\{\phi-\sum_{\nu=1}^{\infty}\eta_\nu Y'_\nu(x_a)\right\}$$

With $k_a/m_a=\omega_a^2$ as the square of the natural circular frequency of the accelerometer, and $c_a/m_a=2\zeta_a\omega_a$, one obtains

$$\ddot{y}_a+2\zeta_a\omega_a\dot{y}_a+\omega_a^2 y_a=-\ddot{y}+x_a\ddot{\phi}$$
$$-\sum_{\nu=1}^{\infty}\ddot{\eta}_\nu Y_\nu(x_a)+g\left[\phi-\sum_{\nu=1}^{\infty}\eta_\nu Y'_\nu(x_a)\right]$$

where ζ_a is the damping factor of the accelerometer.

By scaling the output in such a manner that it is equal to the input, for frequencies small in comparison with the natural frequency of the accelerometer, one has to transform with

$$y_a=-\frac{A_i}{\omega_a^2}$$

where A_i represents the indicated acceleration. The response characteristic of the accelerometer is therefore determined by the differential equation

$$\frac{\ddot{A}_i}{\omega_a^2}+\frac{2\zeta_a}{\omega_a}\dot{A}_i+A_i=\ddot{y}-x_a\ddot{\phi}-g\phi$$
$$+\sum_{\nu=1}^{\infty}\{\ddot{\eta}_\nu Y_\nu(x_a)+g\eta_\nu Y'_\nu(x_a)\} \quad (7.28)$$

Rate Gyro Equation of Motion

In some space vehicles, the rate of the attitude angle, ϕ_i, in the control equation is not obtained by a differentiating network operating on the angle, ϕ_i, but rather by the output signal of a rate gyroscope. The function of a rate gyroscope is to give an output signal which is proportional to the angular velocity about a perpendicular axis. Figure 7.4 represents the

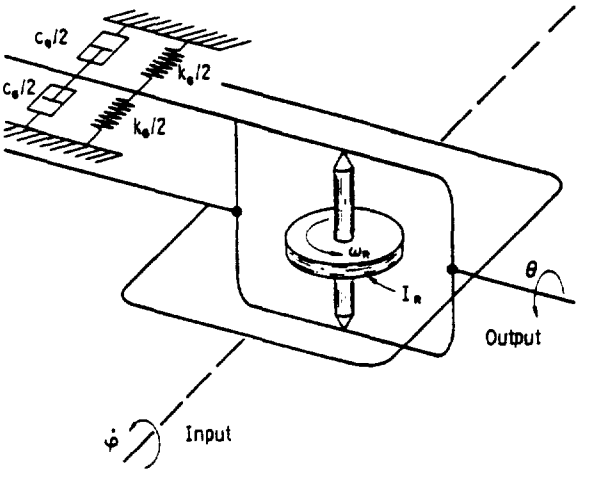

FIGURE 7.4.—Schematic of rate gyroscope mounting.

mounting of such a rate gyroscope. In contrast to the free gyroscope, the outer frame of the rate gyroscope is rigidly fastened to the structure of the vehicle. The inner gimbal support is restrained by a spring and damper which permit a limited rotation about the outer frame. The z-axis about which the vehicle turns is called the input axis, and the axis of rotation of the inner gimbal frame is called the output axis. Any rotation of the vehicle frame at a rate $\dot{\phi}_{iR}$ will act as a forced precession of the spin axis and will induce a gyroscopic reaction torque. This torque is given by

$$M_R=I_R\omega_R\dot{\phi}_R$$

where I_R is the moment of inertia of the rotor and ω_R its angular velocity. $\dot{\phi}_R$ represents the angular velocity of the structure of the vehicle at the location of the rate gyroscope. The torque, M_R, is balanced by the inertial, damping, and restoring moments of the gyroscope about its output axis. Damping has been introduced to prevent the undesirable condition of excessive overshoot and oscillations about the steady-state angle. The behavior of the rate gyroscope can therefore be established from the differential equation

$$I_G\ddot{\theta}+c_G\dot{\theta}+K_G\theta=I_R\omega_R\dot{\phi}_R$$

where I_G represents the moment of inertia of

the rotor and the inner gimbal frame with respect to the output axis. c_G is the coefficient of viscous damping and K_G is the restoring moment per unit angle. By defining

$$\theta = I_R \omega_R \theta_t / I_G \omega_G^2$$

the angle θ is scaled in such a fashion that the indicated value, θ_t, for frequencies small in comparison with the natural frequency, ω_G, of the rate gyroscope ($\omega_G^2 = K_G/I_G$), represents the angular velocity of the vehicle at the location of the gyroscope. The response characteristic of a rate gyroscope of natural circular frequency, ω_G, a damping factor, ζ_G, and an angular velocity, ω_R, of the rotor is therefore described by the differential equation

$$\frac{\ddot{\theta}_t}{\omega_G^2} + \frac{2\zeta_G}{\omega_G}\dot{\theta}_t + \theta_t = \dot{\phi}_R = \dot{\phi} - \sum_{r=1}^{n} \dot{\eta}_r Y_r'(x_R) \qquad (7.29)$$

where θ_t represents the indicated angular velocity of the airframe of the vehicle at the location of the rate gyroscope. The control equation, in which the rate is governed by the output of a rate gyroscope, and with additional accelerometer control, is then (see eq. (7.27))

$$p_2\ddot{\beta} + p_1\dot{\beta} + \beta = a_c\phi_t + a_1\theta_t + g_2 A_t \qquad (7.30)$$

where

$$\phi_t = \phi - \sum_{r=1}^{n} \eta_r Y_r'(x_G) \qquad (7.31)$$

7.3 INFLUENCE OF PROPELLANT LATERAL SLOSHING

The dynamics of space vehicles are best described by the two essential investigations of stability and response. Stability expresses the ability of a system to achieve a state of motion and how rapidly this can be done. In the analysis of space vehicle performance, one usually is satisfied to determine just the roots (boundaries) of stability, rather than solving the total system of equations. The shifting of roots to more optimal positions, if possible, is a major part of the analysis. If this is accomplished, however, the response of the vehicle is then required to determine whether or not the design of the system is appropriate for certain given inputs. In a space vehicle, these design values are the available engine deflection, its rate, maximum bending moments, wave height of the oscillating propellants, etc., as a consequence of a given wind increase and gust through which the vehicle may have to pass during the ascent phase of its flight. The dynamic characteristics of the vehicle differ in complexity depending, of course, upon the complexity of the system itself; they are reduced here to a less complex system by truncating the equations of motion in such a fashion that a more lucid presentation can be provided without loss of the more general features of the system.

Stability Techniques and Stability Boundaries

Since the response of a system depends on its stability, the roots of the system are the most basic parameters of the system dynamics. These describe the response resulting from any excitation and depend only on the physical parameters of the system. We shall therefore discuss, in this section, the basic techniques for obtaining the characteristic roots of a dynamic system and shall study the variation of these stability roots with changes in the physical characteristics of the vehicle.

The optimization of the response behavior of the vehicle is based upon the possibility of shifting the stability roots of the system. (See fig. 7.5.) This means that if the location of the roots can be changed in the complex plane (root locus plane) (fig. 7.5) in such a fashion that they exhibit a larger negative real

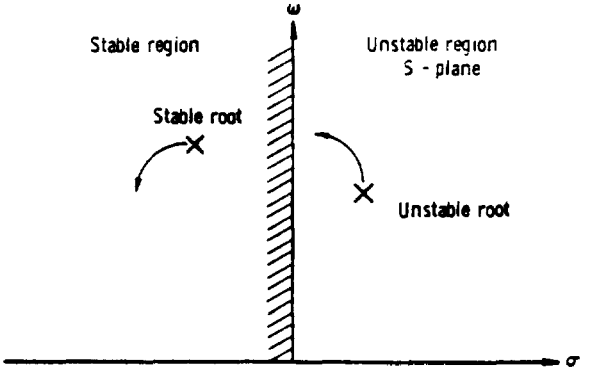

Arrow indicates increasing stability by changing physical parameters of the system (root migration)

FIGURE 7.5.—Root locus plane.

part, by changing the physical properties of the system, the system will show enhanced stability and will more efficiently achieve a steady-state condition and absorb a disturbance more rapidly. A very convenient way to study the migration of stability roots is by plotting them as continuous functions in the complex plane; this is called a root locus plot and represents a curve of all (or those which we are most interested in) root locations in the complex plane $(\sigma+i\omega)$ corresponding to the change of some of the physical parameters of the space vehicle. The effect of the change of any other parameter can also be obtained. One can therefore investigate the necessary changes that should be introduced into the system to yield enhanced stability and response features.

In space vehicles, the characteristic equation is of higher order and a direct analytical solution is laborious and sometimes even unnecessary for design purposes. Although the solution of such a polynomial can be performed by the method of Sturm and Graeffe (ref. 7.10), or its modification by Brodetsky and Smeal (ref. 7.11) without any difficulties, in many cases it is sufficient to know whether or not the real parts of the roots are negative, thus indicating a decaying motion with increasing time (stable motion) or whether they are positive and represent an unstable motion with increasing amplitude as time increases. When a design parameter is to be considered as a variable, it is especially important to have available criteria for the stability in terms of the roots. Criteria of this type are given by Routh (ref. 7.12) and Hurwitz (ref. 7.13). Another method for the determination of the location of the roots is the root locus method by Nyquist (ref. 7.14). In the following, we shall use only the Hurwitz criteria.

A necessary and sufficient condition that the equation

$$\sum_{\lambda=0}^{n} a_\lambda s^\lambda = 0 \tag{7.32}$$

with real and positive coefficients, a_n, have only roots with negative real parts, is that the a_λ and the values of the determinants, H_r, all be positive. The determinant H_r is of the form:

$$H_r = \begin{vmatrix} a_1 & a_3 & a_5 & a_7 & \cdots \\ a_0 & a_2 & a_4 & a_6 & \cdots \\ 0 & a_1 & a_3 & a_5 & \cdots \\ 0 & a_0 & a_2 & a_4 & \cdots \\ \cdots & \cdots & \cdots & \cdots & \cdots \\ 0 & \cdots & \cdots & \cdots & \cdots \end{vmatrix} \tag{7.33}$$

or

$$H_1 = a_1;\ H_2 = \begin{vmatrix} a_1 & a_3 \\ a_0 & a_2 \end{vmatrix};$$

$$H_3 = \begin{vmatrix} a_1 & a_3 & a_5 \\ a_0 & a_2 & a_4 \\ 0 & a_1 & a_3 \end{vmatrix} \tag{7.34}$$

and

$$H_n = a_n H_{n-1} = \begin{vmatrix} a_1 & a_3 & a_5 & \cdots \\ a_0 & a_2 & a_4 & \cdots \\ 0 & a_1 & a_3 & \cdots \\ 0 & a_0 & a_2 & \cdots \\ \cdots & \cdots & \cdots & \cdots \end{vmatrix}$$

For a quadratic equation in s, these conditions are satisfied if the coefficients a_0, a_1, and a_2 are positive. For a cubic equation, the Hurwitz conditions are

$$H_1 = a_1 > 0,\ H_2 = \begin{vmatrix} a_1 & a_3 \\ a_0 & a_2 \end{vmatrix} > 0,$$

and

$$H_3 = \begin{vmatrix} a_1 & a_3 & 0 \\ a_0 & a_2 & a_4 \\ 0 & a_1 & a_3 \end{vmatrix} > 0 \tag{7.35}$$

To obtain some insight into the degree of stability, that is, the rapidity of decay of the motion, it is sometimes of interest to determine

the magnitude of the smallest negative real part. For this reason, one shifts the imaginary axis toward the left by

$$s=\bar{s}-\bar{\sigma}$$

where $\bar{\sigma}>0$ and real. If the transformed polynomial is just still stable, that is, the smallest root is very close to the shifted imaginary axis, we obtain a measure of the magnitude of stability.

The stability boundaries are characterized by the roots, of which at least one has a zero real part while the others are stable roots. For an nth-degree polynomial the stability boundaries are presented by

$$a_n=0 \text{ and } H_{n-1}=0$$

To determine which side of the stability boundary represents the stable region, one point (not located on the boundary) is chosen, and its stability is investigated with the previous Hurwitz determinants, $H_\nu>0$ (eq. (7.35)). For a quadratic equation, the stability boundaries are given by $a_2=0$ and $a_1=0$. For a cubic equation, the conditions are

$$a_3=0 \text{ and } H_2=a_1a_2-a_0a_3=0$$

and for a quartic equation they are

$$a_4=0 \text{ and } H_3=0, \text{ i.e., } a_1a_2a_3=a_1^2a_4+a_0a_3^2$$

Another method for determining the stability would be that of the locus curve. The polynomial of the complex variable, s, represents a complex value, w

$$w=P(s)$$

If all roots, s, are stable roots, they must be located in the left half plane of s, that is, the imaginary axis, $s=i\omega$, separates the left stable from the right unstable region of the $s=\sigma+i\omega$-plane. Introducing $s=i\omega$ into the polynomial $w=P(s)$ and investigating the mapping of this imaginary axis in the w-plane should yield some criteria for the stability of the roots of the polynomial. With

$$s=i\omega$$

and

$$P(s)=\sum_{\lambda=0}^{n} a_\lambda s^\lambda$$

we have

$$w=P(i\omega)=\sum_{\lambda=0}^{[n/2]}(-1)^\lambda a_{2\lambda}\omega^{2\lambda}$$

$$+i\sum_{\lambda=0}^{[n/2]}(-1)^\lambda a_{2\lambda+1}\omega^{2\lambda+1}=X(\omega)+iY(\omega)$$

where $[n/2]$ means the smaller integer closest to $n/2$, or equal $n/2$, if n is even. This indicates that for even n the expression $X(\omega)$ will be an even polynomial of nth degree while $Y(\omega)$ is an odd polynomial of $(n-1)$st degree. For an odd value n, the $X(\omega)$ is an even function of $(n-1)$st degree and $Y(\omega)$ is an odd polynomial of nth degree. Therefore, $X(\omega)=X(-\omega)$ and $Y(\omega)=-Y(-\omega)$. The function $w(\omega)$ is represented in the w-plane locus curve as ω assumes the values from $-\infty$ to $+\infty$. All roots of the polynomial $w=P(s)=0$ are mapped into the origin $w=0$ of the w-plane. The location of this point, therefore, with respect to the locus curve will be characteristic for the root, s_ν, with respect to the imaginary axis. The fact that $X(\omega)$ is even and $Y(\omega)$ is odd reveals that only $\omega\geq 0$ has to be considered. The locus curve starts out for $\omega=0$ on the X-axis and the w-plane at $w=a_0$ and represents, with $\omega\to\infty$, a curve such as shown in figure 7.6. In order to answer now the question of stability of the roots, s_ν, we imagine a point, $s=i\omega$, on the imaginary axis of the s-plane and consider the connecting lines of the νth roots, s_ν, to

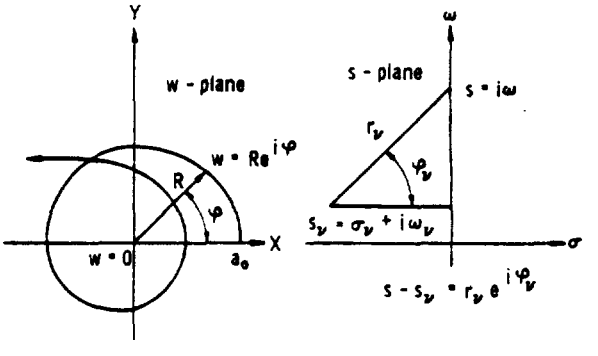

FIGURE 7.6.—Locus-curve method.

that point. This is, however, a factor of the product representation of the polynomial

$$w=P(s)=a_n \prod_{\nu=1}^{n} (s-s_\nu)=a_n\left(\prod_{\nu=1}^{n} r_\nu\right) e^{i\sum_{\nu=1}^{n}\phi_\nu}=Re^{i\phi}$$

where

$$w=X+iY$$
$$X=R\cos\phi$$
$$Y=R\sin\phi$$

From this, one obtains

$$R=a_n \prod_{\nu=1}^{n} r_\nu$$

$$\phi=\sum_{\nu=1}^{n}\phi_\nu$$

If none of the roots, s_ν, is located on the imaginary axis, i.e., $r_\nu\neq 0$, and if $a_n>0$, it follows that $R>0$, which means that X and Y have the same zeros as $\cos\phi$ and $\sin\phi$, respectively. If all roots, s_ν, are in the left-hand plane (stable roots), then ϕ_ν can cover only the angular region from $-\pi/2$ to $+\pi/2$ for $s=i\omega$ moving on the imaginary axis. The angle, ϕ, therefore, can only cover the angular region $-n\pi/2$ to $+n\pi/2$; or, for $\omega=0$ to ∞, it will cover the angular region 0 to $n\pi/2$. The angle, ϕ, is the angle of the complex value $w=Re^{i\phi}$ of the locus curve, and one now obtains the criterion:

> The equation $P(s)=0$ has only roots with negative real part, if the locus curve $w=P(s)=w(\omega)$ (for $s=i\omega$) circles the origin $w=0$ in such a fashion, that the angle, ϕ, covers the angular region from 0 to $n\pi/2$ as ω changes from 0 to ∞ (counting positive toward the left).

If one root is in the positive half plane, say on the real axis, then the angle covers the region from π to $\pi/2$, in rotating by $\pi/2$ in the negative sense. For λ stable and μ unstable roots, the angle, ϕ, yields a rotation of $(\lambda-\mu)\pi/2=m\pi/2$ in the positive sense, if ω ranges from 0 to ∞. With n as the total number of roots

$$\lambda+\mu=n$$

$$\lambda-\mu=m$$

one concludes:

The polynomial of nth degree $P(s)=0$ has

$$\lambda=\frac{n+m}{2} \text{ stable roots}$$

and

$$\mu=\frac{n-m}{2} \text{ unstable roots}$$

if the locus curve for $\omega=0$ to ∞ covers the angular region from 0 to $(\lambda-\mu)\pi/2$ in the positive sense.

This method is particularly useful for investigating the effects of changes in physical parameters on the behavior of a dynamic system, especially if high-speed computing machines are available.

General Criteria for Stability of Vehicle With No Propellant Sloshing

After the equations of motion have been formulated, as indicated in the preceding sections, a dynamic analysis of the vehicle in flight must be performed. The interaction of the bending of the flexible vehicle with the rigid body motion, the sloshing of the propellants, the reaction of the swivel engines and their compliance, the excitations provided by aerodynamic forces and wind gusts, and the coupling of the control system providing the stability of the space vehicle, must all be taken into account. The equations of motion have been linearized and can be solved on a high-speed computer. It is evident that a detailed formulation and dynamic analysis is beyond the scope of this monograph; however, it is possible to discuss more or less simplified sets of equations of motion which shall serve to illustrate gross effects and yet be of fundamental importance in the preliminary design of a space vehicle.

In order to maintain stable conditions throughout powered flight, it is necessary to avoid adverse feedback conditions arising from inherent phase lags of the sensing element and erroneous signals from bending vibrations. Especially for aerodynamically unstable vehicles, which are particularly sensitive to atmospheric disturbances, artificial stabilization through the control system (with accelerometer)

can alleviate the required control deflections of the gimbal engines, and reduce the loads which can be a potential hazard to the flight performance of the vehicle. We will consider here the problem of rigid and flexible vehicles, where the propellant is treated as rigid mass, and determine some of the basic requirements for the location of the sensors and their vibrational characteristics. Some criteria can be developed which yield enhanced stability of the vehicle without resorting to electrical filter networks, as is performed in a complete root locus analysis of the dynamic system. The sensors treated here comprise accelerometers and rate gyroscopes. With these assumptions, the equations of motion, considering only one bending mode, reduce to the following form:

Translational motion: Equation (7.16)

$$m\ddot{y}=F\phi+F_2\beta-F\eta Y'(x_E) \tag{7.36}$$

where Y is the first bending mode.

Pitching motion: Equation (7.17)

$$I\ddot{\phi}+F_2x_E\beta=F\{x_E\eta Y'(x_E)-\eta Y(x_E)\} \tag{7.37}$$

Lateral bending vibration: Equation (7.22)

$$\ddot{\eta}+g_B\omega_B\dot{\eta}+\omega_B^2\eta=\frac{F_2}{M_B}Y(x_E)\beta \tag{7.38}$$

The dynamic characteristics of the control sensors are represented by the following equations:

Accelerometer: Equation (7.28)

$$\frac{\ddot{A}_i}{\omega_a^2}+\frac{2\zeta_a}{\omega_a}\dot{A}_i+A_i=\ddot{y}-x_a\ddot{\phi}-g\phi+\ddot{\eta}Y(x_a)+\eta gY'(x_a) \tag{7.39}$$

Rate gyro: Equation (7.29)

$$\frac{\ddot{\theta}_i}{\omega_G^2}+\frac{2\zeta_G}{\omega_G}\dot{\theta}_i+\theta_i=\dot{\phi}-\dot{\eta}Y'(x_R) \tag{7.40}$$

The control equation is used in its simplified form

$$p_2\ddot{\beta}+p_1\dot{\beta}+\beta=a_0\phi_i+a_1\begin{Bmatrix}\dot{\phi}_i\\ \theta_i\end{Bmatrix}+g_2A_i \tag{7.41}$$

For a given configuration, the control requirements are strongly dependent on the mutual settings of the control system.

In the following discussion, numerical results have been presented for a Saturn I-type vehicle for which half of the thrust is available for control purposes (refs. 7.9 and 7.15).

Criteria for Position Gyroscope

This investigation presents the stability boundaries in the (Y'_G, g_B) plane, indicating at what location a gyroscope should be mounted to maintain stability for a certain structural damping g_B and for various gain values and lag coefficients.

The control equation, equation (7.27), was employed with an accelerometer gain value of $g_2=0$, that is, no additional accelerometer control. Neglecting the effect of translational motion and combining the equations for pitching motion, equation (7.37), and bending oscillations, equation (7.38), with the control equation, equation (7.41), leads to the condition that for this system of three homogeneous algebraic equations the coefficient determinant

$$\begin{vmatrix} Is^2\omega_c^2 & F_2x_E & FY(x_E)-Fx_EY'(x_E)\\ 0 & -\dfrac{F_2Y(x_E)}{M_B} & s^2\omega_c^2+g_Bs\omega_c\omega_B+\omega_B^2\\ -(a_0+a_1s\omega_c) & p_2s^2\omega_c^2+p_1s\omega_c+1 & (a_0+a_1s\omega_c)Y'(x_G)\end{vmatrix}=0$$

must vanish. The stability polynomial is of sixth degree. For $p_2=0.0084$ and $p_1=0.05$, it was found that for a gyroscope location close to the antinode, the degree of structural damping usually provided is sufficient to maintain stability. For low bending frequencies the location behind the antinode seems reasonable, but for larger bending frequencies

a location in front of the antinode also yields stability; this is due to the lag terms in the control equation.

If only the bending equation, equation (7.38), is combined with the simple control equation

$$\beta = a_0\phi_t + a_1\dot{\phi}_t$$

where

$$\phi_t = -\eta Y'(x_G)$$

the stability polynomial is of second order and exhibits stability if the coefficients are positive, and is of the form

$$s^2\omega_c^2 + s\omega_c\left[g_B\omega_B + \frac{F_2Y(x_E)Y'(x_G)}{M_B}a_1\right] + \left[\omega_B^2 + \frac{F_2Y(x_E)Y'(x_G)}{M_B}a_0\right] = 0$$

Since all of the values in these coefficients are positive by their very nature except for $Y'(x_G)$, which can be either positive or negative, the system definitely exhibits stability for $Y'(x_G) > 0$, that is, for a positive bending mode slope at the location of the gyroscope. This means that the gyroscope should be located behind the antinode in the aft section of the vehicle. The stability boundary is at

$$Y'(x_G) = -\frac{M_B g_B \omega_B}{F_2 Y(x_E) a_1}$$

that is, slightly forward of the antinode.

Criteria for Rate Gyroscope

We shall consider the stability criteria for a rate gyroscope by dividing our investigation into two parts: one in which the vehicle is considered as a rigid body, and the other in which the flexibility of the vehicle is described by the fundamental bending mode.

Rigid Body Stability

Treating the equation for pitching motion, equation (7.37), together with the rate gyroscope equation, equation (7.40), together with the simple control equation in its ideal form

$$\beta = a_0\phi_t + a_1\theta_t$$

and assuming again time dependency of the form $e^{s\omega_c t}$, the stability polynomial is obtained by setting the coefficient determinant equal to zero. Thus

$$\begin{vmatrix} Is^2\omega_c^2 & 0 & F_2x_E \\ -s\omega_c & \dfrac{s^2\omega_c^2}{\omega_G^2} + \dfrac{2\zeta_G\omega_c}{\omega_G}s + 1 & 0 \\ -a_0 & -a_1 & 1 \end{vmatrix} = 0$$

which yields a fourth-order stability polynomial:

$$\sum_{\lambda=0} B_\lambda s^\lambda = 0$$

with the coefficients

$$B_4 = 1,\ B_2 = \frac{\omega_c^2}{\omega_G^2} + \frac{a_0F_2x_E}{I\omega_c^2},\ B_0 = \frac{a_0F_2x_E\omega_G^2}{I\omega_c^4},$$

$$B_3 = \frac{2\zeta_G\omega_G}{\omega_c},\ B_1 = \frac{F_2x_Ea_1\omega_G^2}{I\omega_c^3} + \frac{2\zeta_G\omega_Ga_0x_EF_2}{I\omega_c^3}$$

with

$$\omega_c^2 = \frac{gx_E\epsilon a_0}{k^2}$$

and

$$\frac{gx_Ea_1\epsilon}{k^2} = 2\zeta_c\omega_c$$

where

$$\epsilon g = \frac{F_2}{m},\ g = \frac{F}{m}$$

is the longitudinal acceleration of the vehicle and $k^2 = I/m$ is the square of the radius of gyration. This yields

$$B_4 = 1,\ B_2 = 1 + \frac{\omega_c^2}{\omega_G^2},\ B_0 = \frac{\omega_G^2}{\omega_c^2},$$

$$B_3 = \frac{2\zeta_G\omega_G}{\omega_c},\ B_1 = 2\frac{\omega_G}{\omega_c}\left[\zeta_c\frac{\omega_G}{\omega_c} + \zeta_G\right]$$

The stability boundary is obtained by setting $B_1B_2B_3 = B_0B_3^2 + B_4B_1^2$ which leads to

$$\left(\frac{\omega_c}{\omega_G}\right)^2 + \left(\frac{\zeta_c}{\zeta_G}\right)\left(\frac{\omega_c}{\omega_G}\right) - 1 = 0$$

representing a hyperbola in the $\left[\left(\frac{\omega_c}{\omega_G}\right), \left(\frac{\zeta_c}{\zeta_G}\right)\right]$-plane. Only the branch in the first quadrant of the coordinate system is of physical significance and is shown in figure 7.7. The cross-hatched area represents the stable area. From

this we can conclude that rigid body stability can be accomplished by choosing the natural frequency of the rate gyroscope larger than the control frequency and adjust its damping factor to an appropriate value. For a ratio of the damping factors of unity, a frequency ratio range of $0 \leq \frac{\omega_c}{\omega_G} < \left(\frac{\sqrt{5}-1}{2}\right)$ would maintain stability of the rigid vehicle.

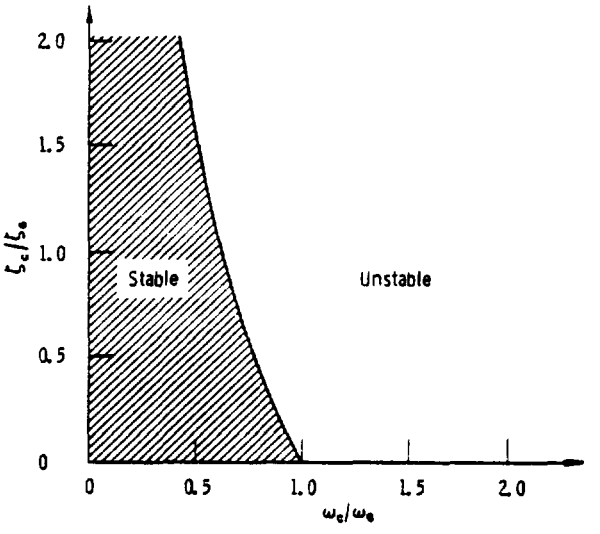

FIGURE 7.7.—Stability boundary for rigid vehicle with rate gyroscope.

Bending Mode Stability

Taking, in this case, the bending equation, equation (7.38), and rate gyroscope equation, equation (7.40), together with the control equation, equation (7.41), while omitting all terms corresponding to rigid body motion, yields the coefficient determinant

$$\begin{vmatrix} s^2\omega_c^2+g_B s\omega_c\omega_B+\omega_B^2 & \frac{-F_2}{M_B}Y(x_B) & 0 \\ s\omega_c Y'(x_R) & 0 & \frac{s^2\omega_c^2}{\omega_G^2}+\frac{2\zeta_G\omega_c s}{\omega_G}+1 \\ a_0 Y'(x_G) & p_2 s^2\omega_c^2+p_1 s\omega_c+1 & -a_1 \end{vmatrix} = 0$$

The stability polynomial, which is of sixth degree, is reduced to a quartic by setting the phase through making the coefficients $p_2=p_1=0$, which yields finally the stability boundary

$$\epsilon'_R = 0$$

and

$$\epsilon'_G+\left(\frac{\zeta_c}{\zeta_G}\right)\left(\frac{\omega_c}{\omega_G}\right)\epsilon'_R-\left(\frac{\omega_G}{\omega_c}\right)^2\left[1-\left(\frac{\omega_B}{\omega_G}\right)^2\right]=0$$

where

$$\epsilon'_G \equiv \frac{Y(x_B)Y'(x_G)}{\frac{M_B}{m}}|x_{c_1R}|$$

and

$$\epsilon'_R \equiv \frac{Y(x_B)Y'(x_R)}{\frac{M_B}{m}}|x_{c_1R}|$$

The value $|x_{c_1R}|$ represents the distance between the center of instantaneous rotation and the mass center of the vehicle.

In the $(\epsilon'_R, \epsilon'_G)$-plane, as shown in figure 7.8, this represents a family of straight lines. The distance of the intersection point with the axis from the origin is decreased by increasing the frequency ratio (ω_B/ω_G), that is, by decreasing the rate gyroscope frequency toward the bending frequency. The slope of the stability boundary line decreases with decreasing damping ratio (ζ_c/ζ_G) and increasing frequency ratio (ω_c/ω_G). Since the frequency ratio is limited to a small value because of the rigid body stability, the slope is most effectively changed by the damping ratio. This indicates that a supercritical damping of the rate gyroscope is desirable. A further conclusion that can be drawn from figure 7.8 with regard to the proper location of the rate gyroscope is that positive slope $Y'(x_R)$ minimizes stability.

Therefore, it can be concluded that the natural frequency for the rate gyroscope should be quite large compared with the control frequency and the highest to-be-controlled bending frequency under consideration. The

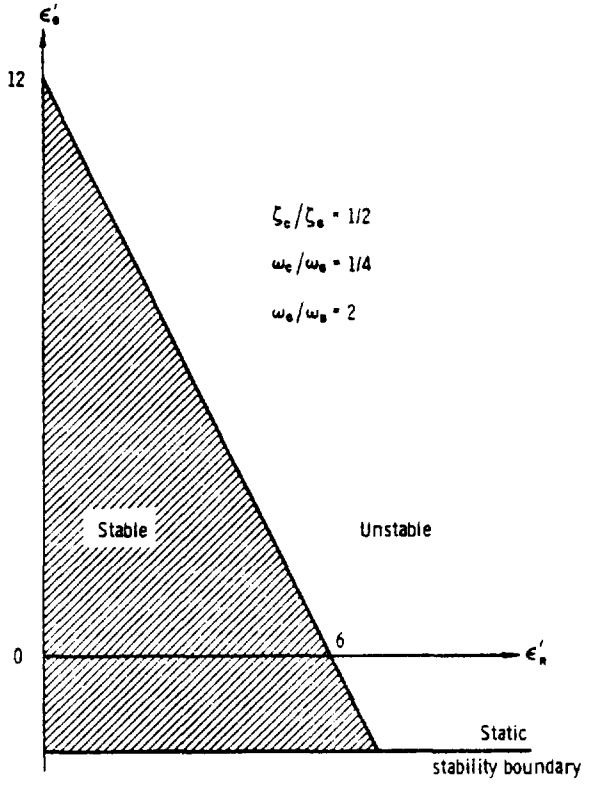

FIGURE 7.8.—Stability boundary for flexible vehicle with rate gyroscope.

damping should preferably be supercritical, or large in comparison with the control damping. Furthermore, the rate gyroscope should be located behind the last antinode of the to-be-controlled bending modes.

Criteria for Accelerometer

In many vehicles, an accelerometer is used as an additional control element. By proper choice of its gain value in the control equation and its vibrational characteristics, such an element can help to diminish loads on the space vehicle and to reduce deflection requirements of the swivel engines. In this section, therefore, we shall investigate the effect of the vibrational characteristics and the gain value g_2 of an accelerometer and shall try to determine simple criteria for the preliminary determination of those values (ref. 7.16).

Rigid Body Stability

Since the translational motion of the vehicle is sensed by an accelerometer, this has to be considered in a simplified stability analysis. Therefore, for rigid body stability, we treat the translational motion, equation (7.36), together with the pitching motion, equation (7.37), the accelerometer equation, equation (7.39), and the control equation, equation (7.41), together with the usual assumption $e^{s\omega_c t}$ for the solution. The coefficient determinant that has to vanish yields, with $\eta=0$, $\phi_t=\phi$ and the phase coefficients $p_1=p_2=0$, the expression

$$\begin{vmatrix} ms^2\omega_c^2 & -F \\ 0 & Is^2\omega_c^2 \\ -s^2\omega_c^2 & (x_c s^2\omega_c^2+g) \\ 0 & -(a_0-s\omega_c a_1) \end{vmatrix}$$

The stability polynomial is of fourth degree with the coefficients

$$B_4=1$$

$$B_3=2\left\{\zeta_a\frac{\omega_a}{\omega_c}+\zeta_c\right\}$$

$$B_2=1+\frac{\omega_a^2}{\omega_c^2}+4\zeta_a\zeta_c\frac{\omega_a}{\omega_c}-\epsilon g g_2\frac{\omega_a^2}{\omega_c^2}\left[1+\frac{x_a x_E}{k^2}\right]$$

$$B_1=2\frac{\omega_a}{\omega_c}\left[\zeta_a+\zeta_c\frac{\omega_a}{\omega_c}\right]$$

$$B_0=\frac{\omega_a^2}{\omega_c^2}$$

$$\begin{vmatrix} 0 & -F_2 \\ 0 & F_2 x_E \\ \dfrac{\omega_c^2 s^2}{\omega_0^2}+\dfrac{2\zeta_a\omega_c s}{\omega_a}+1 & 0 \\ -g_2 & 1 \end{vmatrix}=0$$

The stability condition, with $B_1B_2B_3\geq B_0B_3^2+B_4B_1^2$ and $|x_{c1R}|=k^2/x_E$, is then given by

$$\left(\frac{\zeta_c}{\zeta_a}\right)\left(\frac{\omega_c}{\omega_a}\right)^4+4\zeta_c^2\left(\frac{\omega_c}{\omega_a}\right)^3+\left(\frac{\omega_c}{\omega_a}\right)^2\left\{4\zeta_c^2\left(\frac{\zeta_c}{\zeta_a}\right)+4\zeta_a\zeta_c-2\left(\frac{\zeta_c}{\zeta_a}\right)-\epsilon g g_2(1+\alpha)\left(\frac{\zeta_c}{\zeta_a}\right)\right\}+\left(\frac{\omega_c}{\omega_a}\right)\left\{4\zeta_c^2-\epsilon g g_2(1+\alpha)\left[1+\left(\frac{\zeta_c}{\zeta_a}\right)^2\right]\right\}+\left(\frac{\zeta_c}{\zeta_a}\right)[1-\epsilon g g_2(1+\alpha)]\geq 0$$

This is a polynomial of fourth degree in ω_c/ω_a.

A case of special interest is the ideal accelerometer for which $\omega_a >> \omega_c$. With $\alpha \equiv x_a/|x_{c1R}|$, the result of the above equation with $egg_2=\lambda$, yields the simple expression ($|x_{c1R}|$ is the distance of the center of instantaneous rotation from the mass center)

$$\lambda=\frac{1}{1+\alpha}$$

which is shown in figure 7.9. From this it can be concluded that an accelerometer should be located forward of the center of instantaneous rotation to allow all possible gain values $\lambda(>0)$. With decreasing gain values λ, the location of the accelerometer becomes less important for rigid body stability. Figures 7.10 and 7.11 show the influence of the natural frequency, ω_a, of the accelerometer and of the damping factor, ζ_a. The influence of the change of these parameters is not very pronounced and does not exhibit a large difference from the results for an ideal accelerometer. If the natural frequency of the accelerometer, however, is small (which should be avoided in many respects), the stability boundary curves spread a little more. One can conclude from the above results that a location forward of the mass center will insure stability of the rigid body. With decreasing gain values, the location of the accelerometer becomes less important, indicating that a location aft of the mass center also becomes permissible.

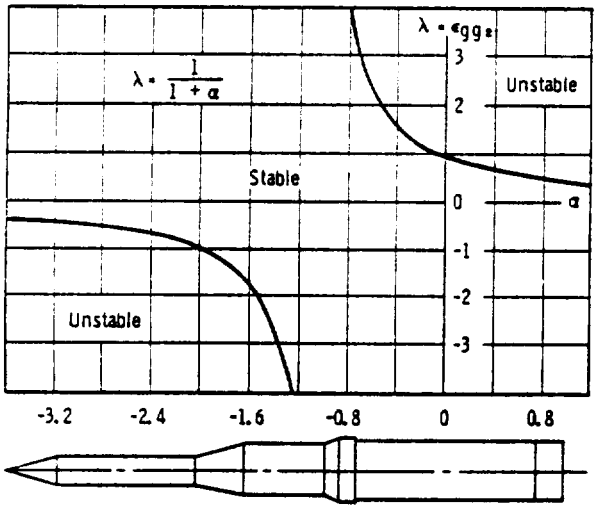

FIGURE 7.9.—Stability boundary for rigid vehicle with ideal accelerometer control.

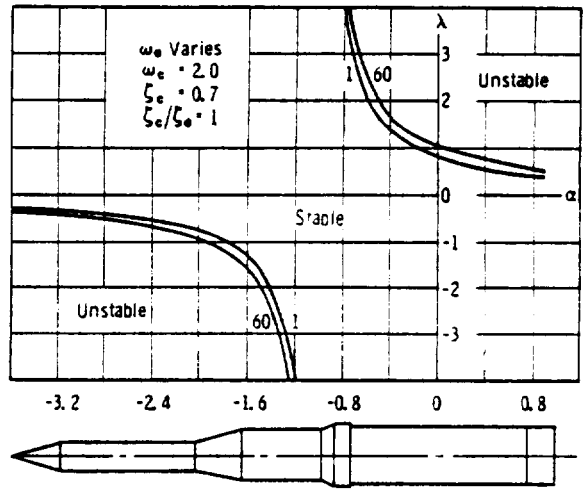

FIGURE 7.10.—Stability boundaries for rigid vehicle with accelerometer control of various natural frequency.

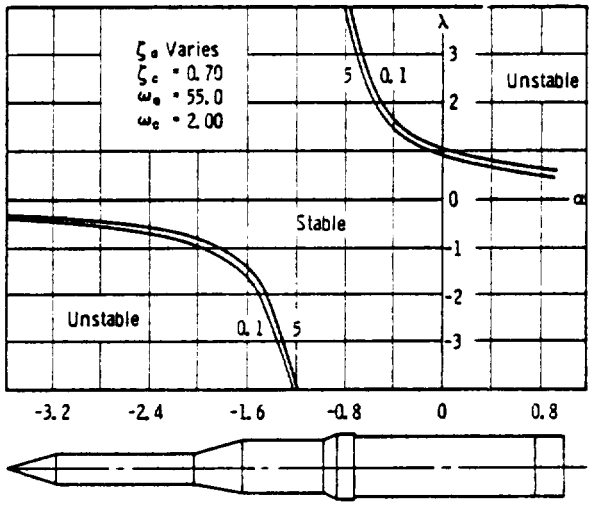

FIGURE 7.11.—Stability boundaries for rigid vehicle with accelerometer control of various damping factor, ζ_a.

It should be mentioned that the expression

$$\omega_c^2=\frac{egx_Ea_0}{k^2}$$

represents the undamped natural frequency of the rigid body (referred to as the control frequency) without accelerometer control. The actual control frequency with accelerometer control depends upon the gain value and loca-

tion of the accelerometer and is given by the expression

$$\omega_{ca}^2=\frac{\epsilon g x_E a_0}{k^2(1-\lambda-\lambda\alpha)}$$

From this it can be seen that a location, x_a, of the accelerometer near the center of instantaneous rotation, that is, $\alpha=-1$, makes the control frequency nearly independent of the gain value, λ. For this value, $\lambda\alpha$, failure of the control accelerometer would therefore not result in an abrupt change of the control frequency and would not drastically influence the stability behavior of the vehicle.

Bending Mode Stability

Considering only the vehicle, equation (7.38), and its interaction with the accelerometer, equation (7.39), and the control equation, equation (7.41), yields the stability determinant

$$\begin{vmatrix} s^2\omega_c^2+g_B\omega_B s\omega_c+\omega_B^2 & -\frac{F_2}{M_B}Y(x_E) & 0 \\ -[s^2\omega_c^2 Y(x_a)+gY'(x_a)] & 0 & \frac{s^2\omega_c^2}{\omega_a^2}+\frac{2\zeta_a\omega_c s}{\omega_a}+1 \\ (a_0+a_1 s\omega_c)Y'(x_G) & p_2\omega_c^2 s^2+p_1\omega_c s+1 & -g_2 \end{vmatrix}=0$$

The stability polynomial is of sixth degree. Assuming, for reasons of simplification as before, that the phase-lag coefficients vanish, that is, $p_1=p_2=0$, the stability polynomial reduces to one of fourth degree. The coefficients are given by

$$B_4=1$$

$$B_3=2\zeta_a\frac{\omega_a}{\omega_c}+2\epsilon'_G\zeta_c$$

$$B_2=\frac{\omega_B^2+\omega_a^2}{\omega_c^2}-\lambda\epsilon_a\frac{\omega_a^2}{\omega_c^2}+\epsilon'_G\left(1+4\zeta_c\zeta_a\frac{\omega_a}{\omega_c}\right)$$

$$B_1=2\zeta_a\frac{\omega_a}{\omega_c}\left[\frac{\omega_B^2}{\omega_c^2}+\epsilon'_G\right]+2\zeta_c\epsilon'_G\frac{\omega_a^2}{\omega_c^2}$$

$$B_0=\frac{\omega_B^2\omega_a^2}{\omega_c^4}-\epsilon'_a\lambda\frac{\omega_a^2}{\omega_c^2 a_{0\epsilon}}+\epsilon'_g\frac{\omega_a^2}{\omega_c^2}$$

where

$$\epsilon_a=\frac{Y(x_E)Y(x_a)}{\frac{M_B}{m}}$$

and

$$\epsilon'_a=\frac{Y(x_E)Y'(x_a)}{\frac{M_B}{m}}\,|x_{c|R}|$$

For an even more simple criterion, let us assume that the position gyroscope is mounted at the antinode of the bending mode, that is, at the location where the slope of the bending mode vanishes ($\epsilon'_G=0$). With this assumption, the coefficients of the stability polynomial yield

$$B_4=1$$

$$B_3=2\zeta_a\frac{\omega_a}{\omega_c}$$

$$B_2=\frac{\omega_B^2+\omega_a^2}{\omega_c^2}-\lambda\epsilon_a\frac{\omega_a^2}{\omega_c^2}$$

$$B_1=2\zeta_a\frac{\omega_B^2\omega_a}{\omega_c^2}$$

$$B_0=\frac{\omega_B^2\omega_a^2}{\omega_c^4}-\frac{\lambda\epsilon'_a}{a_{0\epsilon}}\frac{\omega_a^2}{\omega_c^2}$$

The static stability limit is established from the coefficient B_0, which yields

$$\epsilon'_a\leq\frac{\omega_B^2 a_{0\epsilon}}{\omega_c^2\lambda}$$

where the equal sign expresses the boundary. In the (ϵ_a, ϵ'_a)-plane, this represents a line parallel to the ϵ_a-axis and with a distance from the ϵ_a-axis which increases with the increase of the frequency ratio ω_B/ω_c, the bending frequency over the control frequency (without accelerometer). With increasing attitude gain value, a_0, this boundary shifts farther away from the ϵ_a-axis. Increasing the accelerometer gain, that is, providing more influence of the accelerometer on the control of the vehicle, decreases the distance of the static stability boundary from the ϵ_a-axis. The dynamic stability is expressed by

$$\epsilon'_a\geq a_{0\epsilon}\left(\frac{\omega_B}{\omega_c}\right)^2\epsilon_a$$

where the equal sign represents the stability boundary (fig. 7.12). In the $(\epsilon_a - \epsilon_a')$-plane the stability boundary represents a straight line of slope $a_{0\epsilon}\left(\frac{\omega_B}{\omega_c}\right)^2$ through the origin. Stability is therefore provided below the parallel line to the ϵ_a-axis (static stability boundary) and to the left of the straight line (dynamic stability boundary). With increasing attitude control gain, $a_{0\epsilon}$, the dynamic stability boundary rotates toward the ϵ_a'-axis, providing a large part of the left half plane for stability; in addition, the static stability boundary moves upward. This expresses that a limited range for the location along the vehicle can be provided for the mounting of a control accelerometer. If ϵ_a is negative, that is, the accelerometer is mounted at a location where the bending mode exhibits negative values (vehicle normalized to unity at the gimbal station x_B), then positive and negative values for the slope of the bending mode are available for the location of the accelerometer. With increasing frequency ratio of bending to control frequency, the same trend occurs. For an increase of the availability of thrust for control purposes, the static stability boundary remains at its position, while the dynamic stability boundary rotates again toward the vertical. For increasing accelerometer gain, λ, the static stability boundary moves toward the ϵ_a-axis while the dynamic stability boundary remains fixed, which indicates that a more restricted range of locations for the mounting of a control accelerometer is available.

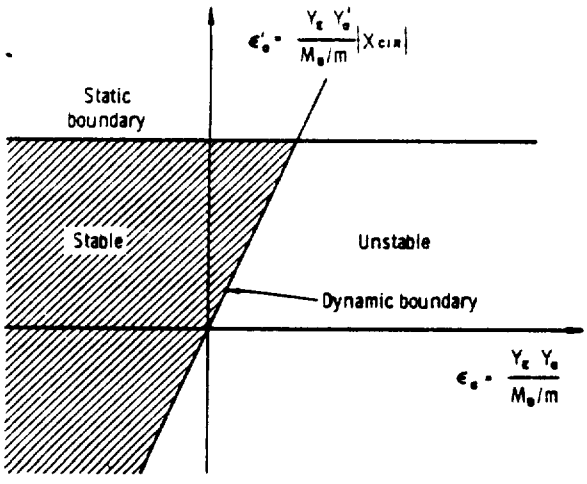

FIGURE 7.12.—Stability boundaries for flexible vehicle with accelerometer control.

Propellant Sloshing in One Container of a Vehicle With Simple Control System

In order to obtain some of the basic effects of the influence of propellant sloshing upon vehicle stability without expending any great numerical effort, the equations of motion of the vehicle will be treated with the propellant as free to oscillate in one container only. The vehicle will be considered as rigid ($\eta_r=0$) and only the most pronounced modal sloshing mass (see ch. 6) will be retained in the analysis; that is, $\lambda=1$ and $n=1$. Introducing $\eta_r=0$ and $n=\lambda=1$ into equations (7.16), (7.17), (7.20), (7.26), and (7.28), one obtains the equations of motion for the rigid vehicle with propellant sloshing in one container and additional accelerometer control (refs. 7.17 and 7.18).

$$m\ddot{y}+m_{11}\ddot{y}_{11}-F\phi-F_2\beta=0 \tag{7.42}$$

$$I\ddot{\phi}-m_{11}x_{11}\ddot{y}_{11}-gm_{11}\ddot{y}_{11}+F_2x_B\beta=0 \tag{7.43}$$

$$\ddot{y}_{11}+2\zeta_{11}\omega_{11}\dot{y}_{11}+\omega_{11}^2y_{11}+\ddot{y}-x_{11}\ddot{\phi}-g\phi=0 \tag{7.44}$$

$$\beta-a_0\phi-a_1\dot{\phi}-g_2A_i=0 \tag{7.45}$$

$$\frac{\ddot{A}_i}{\omega_a^2}+\frac{2\zeta_a}{\omega_a}\dot{A}_i+A_i-\ddot{y}+x_a\ddot{\phi}+g\phi=0 \tag{7.46}$$

The first equation represents translational motions and the second one represents pitching motion of the vehicle. Equation (7.44) is the sloshing equation describing the motion of the first modal sloshing mass. The fourth equation represents the control, which indicates that a position gyroscope and additional accelerometer are employed for the control of the vehicle. Finally, the last equation represents the dynamics of the control accelerometer. If an ideal accelerometer were employed, that is, $\omega_a>>\omega_c$, the first and second terms of equation (7.46) would be neglected. A control system employing no accelerometer control would lead to the omission of the last equation and a vanishing gain value g_2 in equation (7.45). The stability of the solutions of such a system is again obtained by assuming a solution of the

form $e^{s\omega_c t}$, where s is the complex frequency, $s=\sigma+i\omega$. This assumption for the solution transforms the differential equations into a homogeneous algebraic system, which exhibits nontrivial solutions only if the determinants of coefficients vanish. With only the part $F_2=\epsilon F$ available for control purposes, $F_1=(1-\epsilon)F$ and the longitudinal acceleration of the vehicle is $g=F/m$. The coefficient determinant is therefore

$$\begin{vmatrix} (y) & (\phi) & (y_{11}) & (A_1) \\ s^2\omega_c^2 & -g(1+\epsilon a_0+a_1\epsilon\omega_c s) & \mu_{11}s^2\omega_c^2 & -\lambda\epsilon \\ 0 & s^2\omega_c^2+\frac{\epsilon g x_E}{k^2}(a_0+a_1 s\omega_c) & -\frac{\mu_{11}}{k^2}(x_{11}\omega_c^2 s^2+g) & \frac{\lambda x_E \epsilon}{k^2} \\ s^2\omega_c^2 & -(x_{11}\omega_c^2 s^2+g) & \omega_c^2 s^2+2\omega_c\omega_{11}\zeta_{11}s+\omega_{11}^2 & 0 \\ -s^2\omega_c^2 & (x_a\omega_c^2 s^2+g) & 0 & \frac{s^2\omega_c^2}{\omega_a^2}+\frac{2\zeta_a\omega_c s}{\omega_a}+1 \end{vmatrix} = 0 \qquad (7.47)$$

Here, $\lambda=gg_2$ and $\mu_{11}=m_{11}/m$ is the ratio of the sloshing mass in the container to the total mass of the vehicle. The coefficient determinant yields then the characteristic polynomial in s

$$\sum_{i=0}^{6} B_i s^i = 0$$

where the coefficients, B_i, are represented as polynomials of ξ_s and γ_s

$$\begin{aligned} B_6&=k_{17}+k_{18}\xi_s^2 \\ B_5&=k_{13}+2k_{14}\gamma_s+k_{15}\xi_s+k_{16}\xi_s^2 \\ B_4&=k_9+2k_{10}\gamma_s+k_{11}\xi_s+k_{12}\xi_s^2 \\ B_3&=k_6+2k_7\gamma_s+k_8\xi_s \\ B_2&=k_3+2k_4\gamma_s+k_5\xi_s \\ B_1&=k_1+2k_2\gamma_s \\ B_0&=k_0 \end{aligned} \qquad (7.48)$$

The location of the modal mass, $\xi_{11}=x_{11}/k\equiv\xi_s$ (with respect to the mass center), and the damping factor, $\zeta_{11}\equiv\gamma_s$, are extracted, since they are the ones by which the stability of the vehicle can be influenced most readily; the representation of the stability boundaries will be in these coordinates. This therefore yields not only the magnitude of the damping required in the tanks but also its location. The abbreviations $k_j(j=0, 1, 2 \ldots 18)$ depend on the frequency and damping factors, and the gain values of the control system, as well as on the mass ratio, $\mu_{11}\equiv\mu$, and the vibrational characteristics of the accelerometer. With the notations ζ_c as the damping factor of the control system, ω_c as the circular frequency of the control system, $\omega_c^2=\omega_{c0}^2/(1-\lambda\epsilon-\lambda x_E x_a\epsilon/k^2)$ and ω_{c0} as the circular frequency of the control system without accelerometer $(\omega_{c0}^2=gx_E\epsilon a_0/k^2)$, and $\zeta_E=x_E/k$, $\zeta_a=x_a/k$ as the distance with respect to the radius of gyration, and $\nu_s=\omega_s/\omega_c$, $\nu_a=\omega_a/\omega_c$ as the ratios of the eigenfrequencies of sloshing and accelerometer $(\omega_{11}\equiv\omega_s)$ as well as the value $\Lambda=1-\epsilon\lambda(1+\xi_E\xi_a)$, and with

$$a_1=\frac{2\zeta_c a_0}{\omega_c};\quad \frac{gx_E a_1\epsilon}{k^2}=2\zeta_c\omega_c(1-\lambda\epsilon-\lambda\epsilon x_E x_a)$$

the coefficients k_j are given by the expressions:

$$k_0=\Lambda\left[\nu_s^2+\frac{\mu\Lambda}{a_0\epsilon\xi_E^2}\right]$$

$$k_1=2\Lambda\left(\zeta_c+\frac{\zeta_a}{\nu_a}\right)\left[\frac{\mu\Lambda}{a_0\xi_E^2\epsilon}+\nu_s^2\right];\quad k_2=\Lambda\nu_s$$

$$k_3=\Lambda\left\{\frac{1}{\nu_a}\left(\frac{1}{\nu_a}+4\zeta_c\zeta_a\right)\left(\frac{\mu\Lambda}{a_0\xi_E^2\epsilon}+1\right)+1-\mu+\nu_s^2-\frac{\mu\lambda\xi_a}{a_0\xi_E}\right\}$$

$$k_4=2\nu_s\Lambda\left(\zeta_c+\frac{\zeta_a}{\nu_a}\right);\quad k_5=\frac{\mu\Lambda}{a_0\xi_E\epsilon}(a_0\epsilon-1+\lambda\epsilon)$$

$$k_6=2\zeta_a\frac{\nu_s^2}{\nu_a}+\Lambda\left\{\frac{2\mu\zeta_c\Lambda}{a_0\xi_E^2\nu_a^2\epsilon}+2(1-\mu)\frac{\zeta_a}{\nu_a}+2\zeta_c\left(1-\mu-\frac{\nu_s^2}{\nu_a^2}\right)\right\}$$

$$k_7=\Lambda\left\{\nu_s+4\zeta_a\zeta_c\frac{\nu_s}{\nu_a}+\frac{\nu_s}{\nu_a^2}\right\}$$

$$k_8=\frac{2\mu\Lambda}{\nu_a\xi_E}\left\{\zeta_c\nu_a+\zeta_a-\frac{\zeta_a}{a_0\epsilon}\right\}$$

$$k_9=\frac{\nu_s^2}{\nu_a^2}-\epsilon\mu\lambda+\frac{\Lambda(1-\mu)}{\nu_a^2}[1+4\zeta_c\zeta_a\nu_a+\nu_a^2]$$

$$k_{10}=\frac{2\nu_s}{\nu_a^2}[\zeta_c\Lambda+\zeta_a\nu_a]$$

$$k_{11}=\frac{\Lambda\mu}{\xi_E a_0\nu_a^2\epsilon}[a_0\epsilon+4\zeta_c\zeta_a a_0\nu_a\epsilon-1]-\mu\lambda\epsilon(\xi_E+\xi_a)$$

$$k_{12}=\mu(\lambda\epsilon-1);\ k_{13}=\frac{2(1-\mu)}{\nu_a^2}[\zeta_a\nu_a+\zeta_c\Lambda];\ k_{14}=\frac{\nu_s}{\nu_a^2}$$

$$k_{15}=\frac{2\mu\Lambda\zeta_c}{\xi_a\nu_a^2};\ k_{16}=-\frac{2\mu\zeta_a}{\nu_a};\ k_{17}=\frac{1-\mu}{\nu_a^2};\ k_{18}=-\frac{\mu}{\nu_a^2}$$

The various parameters are as follows:

$\mu=m_s/m$=ratio of modal mass of liquid to total mass of space vehicles

ζ_c=control damping factor

$\nu_s=\omega_s/\omega_c$=frequency ratio of undamped propellant frequency to undamped control frequency

γ_s=damping factor of propellant

$\nu_a=\omega_a/\omega_c$=frequency ratio of undamped accelerometer frequency to undamped control frequency

ζ_a=damping factor of the accelerometer

$\lambda=gg_2$=product of longitudinal acceleration of the vehicle and gain value of the accelerometer

$\xi_a=x_a/k$=ratio of the coordinate of the accelerometer location to radius of gyration of the space vehicle

$\xi_s=x_s/k$=ratio of the coordinate of the location of the modal mass of the propellant to radius of gyration of the space vehicle

a_0=gain value of the attitude control system

The stability boundaries are characterized by the roots, s, one of which at least will have a zero real part, while the others are stable roots. The theorem of Hurwitz for a stability polynomial of the nth degree (ref. 7.13)

$$B_n=0,\qquad H_{n-1}=0$$

where H_{n-1} represents the Hurwitz determinant of the form

$$H_{n-1}=\begin{vmatrix} B_1 & B_3 & B_5 & \cdots \\ B_0 & B_2 & B_4 & \cdots \\ 0 & B_1 & B_3 & \cdots \\ 0 & B_0 & B_2 & \cdots \\ \cdots & \cdots & \cdots & \cdots \end{vmatrix}\quad (n-1)\text{ lines and columns}$$

Representing the stability boundaries in the $(\xi_s,\ \gamma_s)$-plane, the Hurwitz determinant $H_5=0$ results in a polynomial

$$\sum_{j=0}^{5} C_j(\xi_s)\gamma_s^j=0$$

where the functions $C_j(\xi_s)$ are polynomia's in ξ_s. The stability boundary for the undamped liquid is $C_0(\xi_s)=0$, and represents the intersection points with the ξ_s-axis. For all points (ξ_s, γ_s) above the stability boundary, one obtains stability. Because of $B_n=0$, the stability is interrupted at the left and at the right so that only within these boundaries is stability guaranteed. The stability boundaries of $B_n=0$ to the right and left are given in the form of straight lines perpendicular to the ξ_s-axis as

$$\xi_s=\pm\sqrt{\frac{k_{17}}{k_{18}}}=\pm\frac{\sqrt{1-\mu}}{\mu}$$

For most vehicles, however, these boundaries play no practical role. Substitution of $\xi_s=\gamma_s=0$ into the Hurwitz determinants determines whether the origin is in the stable or unstable region. A necessary and sufficient condition for stability is (ref. 7.19)

(1) The coefficients:

$B_n,\ B_{n-1},\ B_{n-3}$ ---------->0

$B_1,\ B_0>0$ for even n

$B_0>0$ for odd n

(2) The Hurwitz determinants:

$H_{n-1},\ H_{n-3}$ ---------->0

$H_3>0$ if n is even

$H_2>0$ if n is odd

Rigid Space Vehicle Without Accelerometer Control

Using a simple control system without an accelerometer ($\lambda=0$) results in a stability polynomial of fourth degree. The coefficients B_j would be obtained from equations (7.48) and (7.49) if one introduces $\omega_c=\infty$ and $\lambda=0$, which yields $B_6=B_5=0$. The stability boundaries due to $B_n=0$ are again straight lines given by $\xi_s=\pm\frac{\sqrt{(1-\mu)}}{\mu}$. The stability boundary, from the Hurwitz determinant $H_{n-1}=0$ (here $H_3=0$ or $B_1B_2B_3=B_0B_3^2+B_1^2B_4$), is then given by the expression

$$(K_1+K_2\xi_s+K_3\xi_s^2)+2\gamma_s(K_4+K_5\xi_s+K_6\xi_s^2)+4\gamma_s^2(K_7+K_8\xi_s+K_9\xi_s^2)+8\gamma_s^3=0$$

where

$$K_1=k_1k_3k_6-k_1^2k_9-k_0k_6^2$$

$$K_2=k_1k_5k_6+k_1k_3k_8-2k_0k_6k_8-k_1^2k_{10}$$

$$K_3=k_1k_5k_8-k_0k_8^2-k_1^2k_{11}$$

$$K_4=k_1k_4k_6+k_2k_3k_6+k_1k_3k_9-2k_0k_6k_7-2k_1k_2k_9$$

$$K_5=k_2k_6k_6+k_1k_5k_7+k_1k_4k_8+k_2k_3k_8-2k_0k_1k_8-2k_1k_2k_{10}$$

$$K_6=k_2k_5k_8-2k_1k_2k_{11}$$

$$K_7=k_2k_4k_6+k_1k_4k_7+k_2k_3k_7-k_0k_7^2-k_2^2k_9$$

$$K_8=k_2k_5k_7+k_2k_4k_8-k_2^2k_{10}$$

$$K_9=k_2^2k_{11}$$

$$K_{10}=k_2k_4k_{11}$$

The points of intersection of this stability boundary with the ξ_s-axis are obtained by setting $\gamma_s=0$ and solving the quadratic equation

$$K_1+K_2\xi_s+K_3\xi_s^2=0$$

The roots of this quadratic equation yield

$$\xi_1=-|\xi_d|$$
$$\xi_2=|\xi_d|(1-\mu)/a_0\nu_s^2$$

and give a first estimate for the critical area. The value $1/a_0\nu_s^2$ has been considered to be of small magnitude. This assumption is satisfied in some cases if the control frequency is far enough away from the first natural frequency of the liquid. Therefore, the result expresses that the stability boundary for small values of $1/a_0\nu_s^2$ intersects the ξ_s-axis in the vicinity of the center of mass (origin) and the instantaneous center of rotation $\xi_d=x_d/k$.

One can see that the second point of intersection, ξ_2, becomes sensitive to changes of $1/a_0\nu_s^2$, which indicates that for decreasing gain values, a_0, the intersection point shifts toward the tail of the vehicle. The same behavior occurs if $\nu_s=\omega_s/\omega_c$ decreases. This means that, for a decreasing eigenfrequency of the liquid (or increasing control frequency), damping of the propellant must be provided in a container in the aft section of the vehicle in order to maintain stability. Figure 7.13 indicates that the danger zone for instability of the vehicle is located approximately between the center of gravity and the center of instantaneous rotation. In this zone, the propellant must be more or less damped, depending on the magnitude of the modal mass of the liquid. For

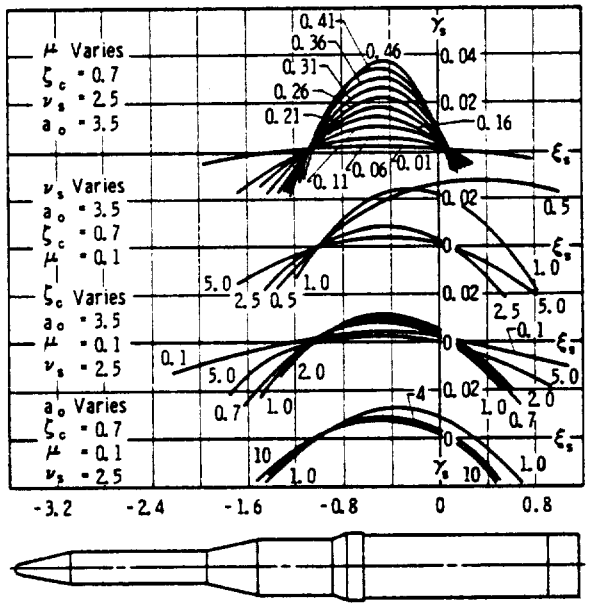

FIGURE 7.13.—Stability boundaries of rigid vehicle with simple control system.

increasing modal mass, more damping is needed in the danger zone. This is most unfavorable if the control frequency is below the natural frequency of the propellant; that is, if $\nu_s<1.0$. For $\nu_s>2$, the wall friction ($\gamma_s=0.01$) alone is sufficient to guarantee stability.

The change of the control damping, ζ_c, indicates that, for increasing subcritical damping, $\zeta_c<1$, the stability in the danger zone will be diminished while, for increased supercritical damping, $\zeta_c>1$, the stability is enhanced. This means that less damping is necessary in the container to maintain stability in the case $\zeta_c>1$. No additional baffles are required in the danger zone if (for a mass ratio $\mu=0.1$) the control damping $\zeta_c\leq 0.5$, or $\zeta_c\geq 2.0$. This indicates that, for these values and the parameters $\nu_s=2.5$ and $a_0=3.5$, the wall friction in the container is sufficient to maintain stability.

Another important question in the design of a large space vehicle is the choice of the form of the propellant containers. We observed in chapter 2 that tank geometry plays an important role in governing the modal masses and the natural frequencies of the propellant. Containers with large diameters exhibit small natural frequencies, which often are too close to the control frequency. Of course, the magnitude of the modal mass considerably emphasizes this unfavorable effect upon the stability. Clustering of numerous smaller containers not only increases the natural frequencies of the propellant (because of the smaller diameters) but also reduces the modal masses, which is a much more important effect. In addition to weight saving and the slight increase of the natural frequencies, subdivision of tanks by sector walls has the advantage of distributing the modal masses to different vibration modes of the liquid. To summarize then, we note that with increasing mass, the stability naturally decreases. The influence of the eigenfrequency change of the propellant with fixed modal mass is such that a decrease of the natural frequency increases the danger zone toward the end of the vehicle and requires more local damping in the propellant. With increasing natural frequency of the liquid, the influence of the propellant sloshing on the stability of the vehicle diminishes more and more. Wall friction alone is then already sufficient to maintain stability.

The gain value, a_0, of the attitude contro system shows, for decreasing magnitude, a decrease of stability in addition to a small enlargement of the danger zone toward the end of the vehicle.

For these numerical results, a Saturn I-type space vehicle of a length of about 170 feet was employed, as before.

Rigid Space Vehicle With Ideal Accelerometer Control (ref. 7.16)

By introducing an additional control element into the control system in the form of an ideal accelerometer ($\omega_a>>\omega_c$), and properly choosing the gain value, g_2, which determines the influence of the accelerometer in the control system, the danger zone can be minimized considerably. Because of $\nu_a>>1$, the coefficients of the stability polynomial are $B_5=B_3=0$, and one obtains again a stability polynomial of fourth degree. The same formulas as in the previous case are valid, except that in the values k_i the appropriate terms with λ have to be considered. The boundaries $B_1=0$ are again straight lines, given by the equation

$$\xi_a=\frac{\frac{1}{4\mu(\epsilon\lambda-1)}\left\{2\mu\lambda\epsilon(\xi_g+\xi_a)\pm\sqrt{4\mu^2\lambda^2\epsilon^2(\xi_g+\xi_a)^2-16\mu(\lambda\epsilon-1)[1-\mu-\lambda\epsilon-\lambda\epsilon(1-\mu)\xi_g\xi_a]}\right\}}{\sqrt{1-\frac{1}{16\mu^2(\epsilon\lambda-1)^2}\left\{2\mu\lambda\epsilon(\xi_g+\xi_a)\pm\sqrt{4\mu^2\lambda^2\epsilon^2(\xi_g+\xi_a)^2-16\mu(\lambda\epsilon-1)[1-\mu-\lambda\epsilon-\lambda\epsilon(1-\mu)\xi_g\xi_a]}\right\}^2}}$$

and are parallel to the γ_s-axis. For values of $\lambda=gg_2<1$, the danger zone is located approximately behind the center of instantaneous rotation and shifts with decreasing gain value g_2 toward a zone between the mass center and the center of instantaneous rotation. The stability decreases, which means more damping in the tank is necessary for increasing $\lambda>1$. This indicates that, for a greater influence of the accelerometer in the control system, the

229-648 O—67——17

danger zone shifts forward of the center of instantaneous rotation and increases with increasing gain value toward the nose of the vehicle (fig. 7.14). For propellant containers in this location, strong damping must be employed to obtain stability. For values of $\lambda=1.5$, the vehicle is unstable if the tank, even with only a 10-percent slosh mass, is located in front of the center of instantaneous rotation, unless additional baffles are provided. For containers behind the center of instantaneous rotation, the vehicle is stable. Furthermore, one recognizes that $\lambda \approx 1.0$ represents the most favorable gain value. In this case, the danger zone shrinks to a small region around the center of instantaneous rotation, in which case the wall friction of the propellant is usually sufficient to provide a stable flight situation.

Changes in the other parameters, such as the slosh mass ratio, μ, the frequency ratio, $\nu_s=\omega_s/\omega_c$, the control system damping, ζ_c, as well as the gain value, a_0, of the attitude system, exhibit the same influences as in the previous case. An enlargement of the danger zone toward the end of the vehicle occurs for large control frequencies and also for small propellant frequencies ($\nu_s<1$), even in the most favorable case in which $\lambda=1.0$.

The addition of an accelerometer introduces another important parameter: its location ξ_a. For $\lambda=1$, the most favorable case for an ideal accelerometer, the influence of its location upon stability of the vehicle is unimportant. For other values of g_2, the location of the accelerometer has considerable influence upon stability. A stronger effect of the accelerometer (say $\lambda>$ 1.5) in the control system and a location in front of the center of mass yields large instability if the container is located behind the center of instantaneous rotation with the accelerometer being in front of the center of mass. Propellant sloshing in those tanks located forward of the center of instantaneous rotation will make the vehicle unstable if the accelerometer is forward of the center of mass. For decreasing values $g_2<1/g$, the stability behavior of the vehicle approaches that of a rigid vehicle without additional accelerometer control. It should, however, be mentioned here that these results are too optimistic, since every accelerometer has its own vibrational characteristics which must be considered.

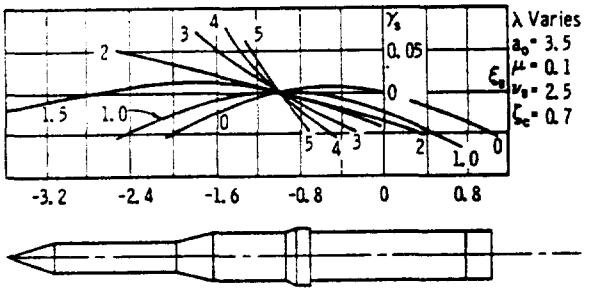

FIGURE 7.14.—Stability boundaries of rigid vehicle with additional ideal accelerometer control (influence of gain value of the accelerometer).

Rigid Space Vehicle With Accelerometer Control of Nonideal Characteristic

The dynamic behavior of an accelerometer, its natural frequency, ω_a, and damping factor, ζ_a, have a nonnegligible influence upon the overall stability of the vehicle. From the results of equations (7.47), (7.48), and (7.49), it is recognized that the stability polynomial is of sixth degree; therefore, the stability boundaries are given by $H_5=0$, and $B_6=0$.

The main influence arises from the natural frequency of the accelerometer. In the numerical evaluation, two circular frequencies ($\omega_a=55$ and 12 rad/sec) were considered for the accelerometer. For decreasing accelerometer frequency, with a damping factor, $\zeta_a=\sqrt{2}/2$, the danger zone increases from the center of instantaneous rotation toward the end of the vehicle (fig. 7.15). The influence of increasing liquid mass has the same effect as previously, with the exception that it is very much amplified for small eigenfrequencies of the accelerometer; a large amount of damping is required in the container in order to obtain stability of the vehicle. For a natural frequency of the accelerometer of $\omega_a=55$ rad/sec, wall friction is in most cases sufficient to maintain stability. For small natural frequencies of the accelerometer, propellant sloshing is excited. This indicates that the situation is more unfavorable with a "bad" accelerometer than in the case without one. The damping required in such a

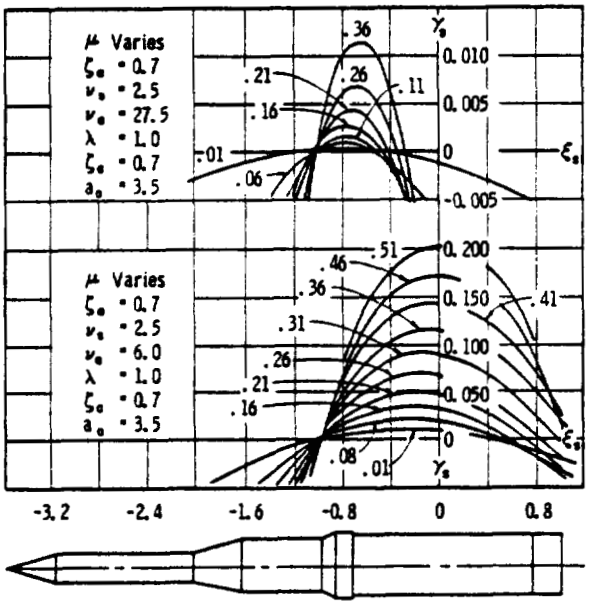

FIGURE 7.15.—Stability boundaries of rigid vehicle with additional accelerometer control of various eigenfrequencies.

case would be about three to four times as much as in the case without additional accelerometer control. The results of the preceding section, and those presented here, indicate that the natural frequency of the accelerometer should be chosen as large as possible. In order to emphasize the influence of the accelerometer characteristics, we consider the effect of the changes of the undamped natural frequency, ω_a, the damping factor, ζ_a, and the coordinate of location, x_a, upon the stability of the vehicle. For increasing natural frequency of the accelerometer $\omega_a < \omega_s$, an increase of the danger zone is obtained, and more damping is required in the container to maintain stability. Above the natural frequency of the propellant, a decrease of the danger zone and enhanced stability can be observed. This means that less damping is required to maintain stability. The larger the frequency ratio $\nu_a/\nu_s = \omega_a/\omega_s$, the less damping is required in the then continuously decreasing danger zone. The influence of the frequency, ω_a, and the damping factor, ζ_a, of the accelerometer is exhibited in figure 7.16. The increase of ζ_a enlarges the danger zone and requires more damping in the propellant container. This effect is more pronounced the smaller the eigenfrequency of the accelerometer. From a damping factor, ζ_a, which is about twice the critical damping or larger, one recognizes, in the case $\omega_a = 12$ rad/sec, that a further increase of the damping factor decreases the danger zone slightly from the back and only slightly enhances the stability. A very important parameter in the design of a control system of a space vehicle is the location, ζ_a, of an accelerometer for control purposes. The influence of this value can be seen in figure 7.17. An accelerometer location aft of the center of gravity of the vehicle must be avoided; shifting the accelerometer toward the nose of the vehicle enhances the stability. An increase in the control frequency, ω_c (fig. 7.18), below the natural frequency of the propellant ($\nu_s > 1$)-increases the danger zone toward the tail of the vehicle. For $\omega_a = 55$ rad/sec (the larger natural frequency of the accelerometer), the required damping in the liquid for maintaining stability of the vehicle is relatively small ($\gamma_s = 0.005$ and less). The influence of the control damping, ζ_c, is given by

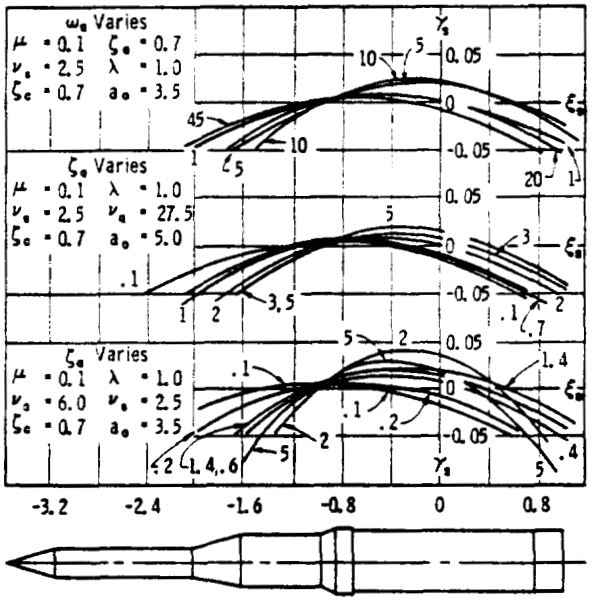

FIGURE 7.16.—Stability boundaries of a rigid vehicle with additional accelerometer control of various vibrational characteristics.

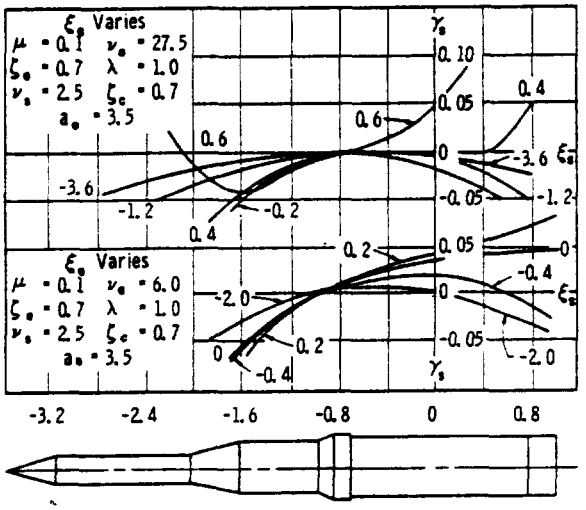

FIGURE 7.17.—Stability boundaries of a rigid vehicle with additional accelerometer control (influence of the location of the accelerometer).

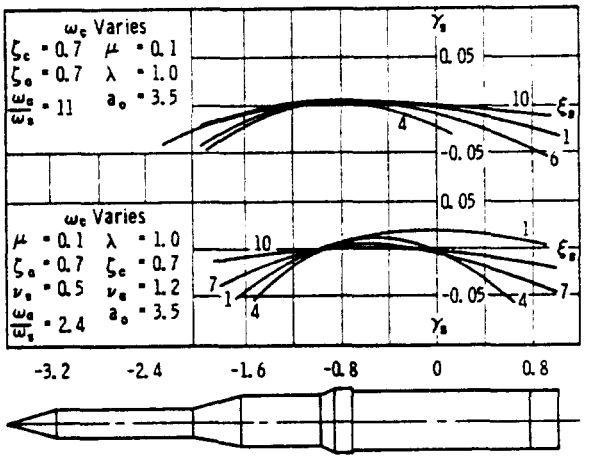

FIGURE 7.18.—Stability boundaries of a rigid vehicle with additional accelerometer control (influence of the control frequency).

the fact that, for increasing subcritical control damping, $\zeta_c < 1$, the danger zone decreases and the stability increases, while for supercritical damping, $\zeta_c > 1$, the stability becomes more unfavorable (fig. 7.19). The influence of the propellant frequency being below the control frequency indicates again the enlarged danger zone which stretches nearly from the center of instantaneous rotation toward the end of the vehicle. Increasing propellant frequency leads

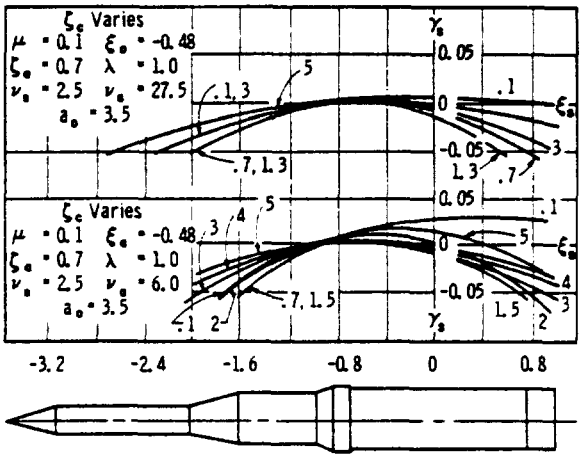

FIGURE 7.19.—Stability boundaries of a rigid vehicle with additional accelerometer control (influence of the control damping).

to a decreasing danger zone and less required damping. Approaching the natural frequency, ω_a, of the accelerometer makes the vehicle more unstable and increases the danger zone toward the end of the vehicle. The gain value, a_0, has only a small influence on the stability; its gain growth increases stability slightly and somewhat decreases the danger zone. Of important influence upon stability is the gain value g_2 of the accelerometer because it presents the strength of the accelerometer in the control system. Figure 7.20 exhibits this influence for

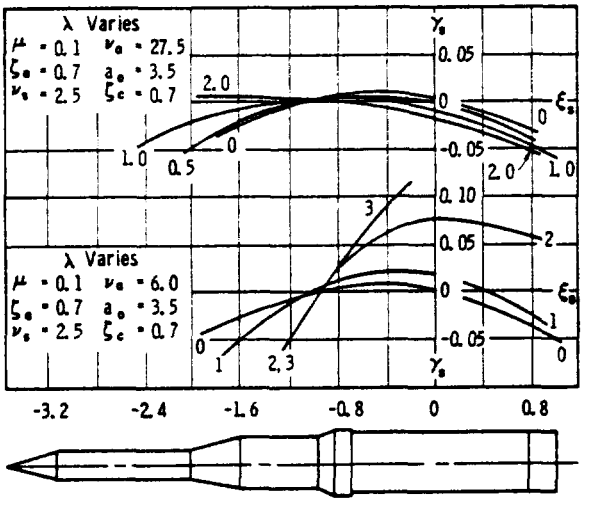

FIGURE 7.20.—Stability boundaries of a rigid vehicle with additional accelerometer control (influence of the gain value of the accelerometer).

two accelerometer frequencies. For an eigenfrequency of the accelerometer of $\omega_a = 55$ rad/sec, one recognized similar behavior as in the case of the ideal accelerometer case, for a value of $\lambda \approx 1.5$. An increase of $\lambda = gg_2$ exhibits an increase in stability and a decrease of the danger zone between the center of instantaneous rotation and the center of mass of the vehicle. For further increase of λ, the danger zone shifts forward of the center of instantaneous rotation. With increasing λ, more damping is required in the propellant container in this zone to maintain stability. For an accelerometer with a small eigenfrequency, the situation is quite different. For increasing gain value g_{2_1}, the stability constantly decreases. Here, the influence of the accelerometer favors instability; it not only increases the danger zone toward the end of the vehicle but it also requires considerably more damping in the propellant tank. It even requires more damping than in the case without accelerometer control ($\lambda = 0$). From this, one can again conclude that large accelerometer frequency is required to stabilize the vehicle with respect to propellant sloshing.

In conclusion, one can state that the danger zone is located between the center of instantaneous rotation and the center of mass, and that it can be diminished by an additional control element in the form of an accelerometer, recognizing that the natural frequency and location have to be properly chosen. These results are valid only for a rigid vehicle in which the sloshing propellant mass in one container is much larger than those in the other tanks. Furthermore, it has to be mentioned that the bending vibration of the vehicle has an effect on the propellant sloshing as well as on the choice of the accelerometer characteristics and its location. If the control frequency and the first bending frequency are sufficiently separated from each other, then the location of an accelerometer requires negative displacement of the bending modes (if the bending modes are normalized at the tail of the vehicle). This indicates that, for the control of the first two bending modes, an approximate location of the accelerometer forward of the center of gravity is appropriate. This location would also be favorable from the standpoint of propellant sloshing.

Effects of Container Geometry and Tank Arrangements

A question of great importance in the design of a large space vehicle is the choice of the form of the propellant containers. As was shown in chapter 2, tank geometry establishes the modal masses and the natural frequencies of the propellant. Containers with large diameters exhibit small natural frequencies that in many cases are too close to the control frequency. The magnitude of the modal mass considerably emphasizes this unfavorable effect upon the stability. Clustering of numerous smaller containers not only increases the natural frequencies of the propellant (because of the smaller diameters) but also reduces the modal masses, of which the latter is a much more important effect on the overall dynamics of the vehicle. In addition to the weight saving and the slight increase of the natural frequencies, subdivision of tanks by sector wall has the advantage of distributing the modal masses to different vibration modes of the liquid.

To summarize the previous results, with increasing mass the stability decreases and the influence of the eigenfrequency change of the propellant of fixed modal mass is such that a decrease of the natural frequency increases the danger zone toward the end of the vehicle and requires more local damping in the propellant. With increasing natural frequency of the liquid, the influence of the propellant sloshing on the stability of the vehicle diminishes more and more. Wall friction is in many cases sufficient to maintain stability.

Clustered Containers

In the case of a cluster of tanks with smaller diameters, the results are very similar. The natural frequency is increased because of the smaller diameters. The natural frequency ratio of the propellants in a single circular cylindrical

tank of radius a, and p identical circular cylindrical tanks of the same total volume, is

$$\frac{f_n^{(1)}}{f_n^{(p)}}=\frac{1}{(p)^{1/4}}\left\{\frac{\tanh\frac{\epsilon_n h}{a}}{\tanh\epsilon_n(p)^{1/2}\frac{h}{a}}\right\}^{1/2}$$

This shows that the frequency increase is proportional only to the slowly increasing value $(p)^{-1/4}$. The total sloshing mass, however, decreases more rapidly with the inverse value of the square root of the number of containers. The ratio of the total sloshing mass of p tanks and the sloshing mass of the single container is

$$\frac{m_s^{(p)}}{m_s^{(1)}}=\frac{1}{p^{1/2}}\frac{\tanh\epsilon_n(p)^{1/2}\frac{h}{a}}{\tanh\frac{\epsilon_n h}{a}}$$

This is of great advantage for the dynamics, but, from the design and overall performance standpoint, the clustering of tanks has structural and weight disadvantages.

The slosh damping required for p clustered tanks is therefore approximately that of a sloshing mass that is reduced by $1/p^{1/2}$. There is, of course, also a small stability enhancing effect because of the increase of the natural frequency.

Rigid Vehicle With Propellant Sloshing in Two and Three Tanks

In some cases the influence of the propellant in other tanks cannot be neglected, making the determination of stability boundaries for vehicles with more sloshing masses mandatory (ref. 7.17). The equations of motion are obtained by treating equations (7.20), (7.42), (7.43), and (7.45) with $\eta_\nu=0$, $\lambda=1, 2, 3$ and/or $n=1, 2$. The propellant will be treated as being free to oscillate in three tanks. This seems to be sufficient, since usually, even in large vehicles, only three of the tanks will exhibit large sloshing masses. The sloshing propellant masses of tanks with light propellants and tanks of smaller diameter can be neglected. With the usual assumption regarding solutions of the form $e^{i\omega_c t}$, where s is the complex frequency, $s=\sigma+i\omega$, the differential equations are transformed into homogeneous algebraic equations, with the characteristic determinant

$$\begin{vmatrix} s^2\omega_c^2 & -g(1+\epsilon a_0+\epsilon a_1 s\omega_c) & \mu_1 s^2\omega_c^2 & \mu_2 s^2\omega_c^2 & \mu_3 s^2\omega_c^2 \\ 0 & s^2\omega_c^2+\frac{\epsilon g x_E}{k^2}(a_0+s\omega_c a_1) & \frac{\mu_1}{k^2}(x_1\omega_c^2 s^2+g) & -\frac{\mu_2}{k^2}(x_2\omega_c^2 s^2+g) & -\frac{\mu_3}{k^2}(x_3\omega_c^2 s^2+g) \\ s^2\omega_c^2 & -(x_1\omega_c^2 s^2+g) & s^2\omega_c^2+2\gamma_1\omega_1\omega_c s+\omega_1^2 & 0 & 0 \\ s^2\omega_c^2 & -(x_2\omega_c^2 s^2+g) & 0 & s^2\omega_c^2+2\gamma_2\omega_2\omega_c s+\omega_2^2 & 0 \\ s^2\omega_c^2 & -(x_3\omega_c^2 s^2+g) & 0 & 0 & s^2\omega_c^2+2\gamma_3\omega_3\omega_c s+\omega_3^2 \end{vmatrix}=0 \tag{7.50}$$

Here, $\mu_\nu=m_\nu/m$ is the ratio of the sloshing mass in the νth container to the total mass of the vehicle. For nontrivial solutions, the coefficient determinant, equation (7.50), must vanish, from which one obtains the characteristic polynomial in s

$$\sum_{i=0}^{8} B_i s^i=0$$

and for which the coefficients B_i depend on the previously mentioned parameters. A similar result is obtained for two containers by removing the last column and line from the above determinant, equation (7.50).

The stability boundaries for four important propellant tank configurations are discussed below:

(1) *Two concentric containers.*—It may be possible to remedy the influence of propellant sloshing by choosing a concentric tank arrangement consisting of an inner tank with circular cross section (radius $r=b$) and an outer tank of annular cross section with an outer radius $r=a$. By proper choice of the diameter ratio

$k=b/a$, the liquid masses in the inside container and outside container can be brought into such a phase relation that the forces and moments of these individual tanks cancel each other. Figures 7.21, 7.22, and 7.23 show the results of this study for diameter ratios $k=b/a=0.3$, 0.5, and 0.7. The results are very similar to those of the case of a single container, since the difference in the location of the sloshing masses is very small. The danger zone is increased somewhat toward the rear of the vehicle. For increasing control damping, ζ_c, the stability is decreased. A decrease in the control frequency enhances the stability, as in the preceding section. For a sloshing frequency of the center tank below the control frequency, more baffling has to be employed over the enlarged danger zone. For increasing sloshing

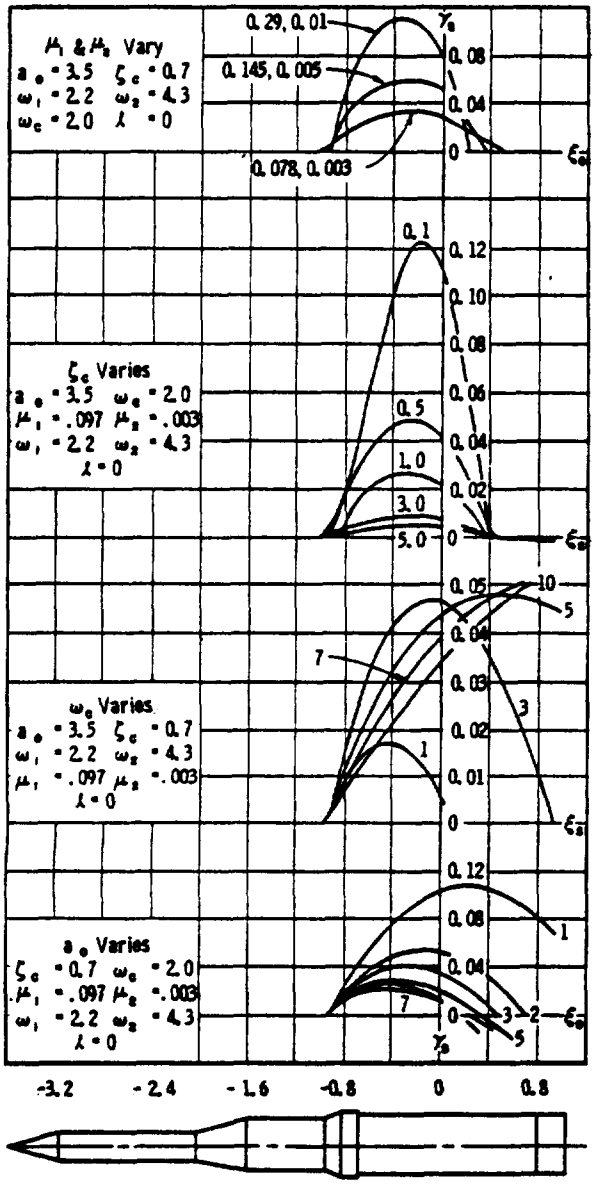

FIGURE 7.21.—Stability boundaries for sloshing in concentric tanks ($k=0.3$).

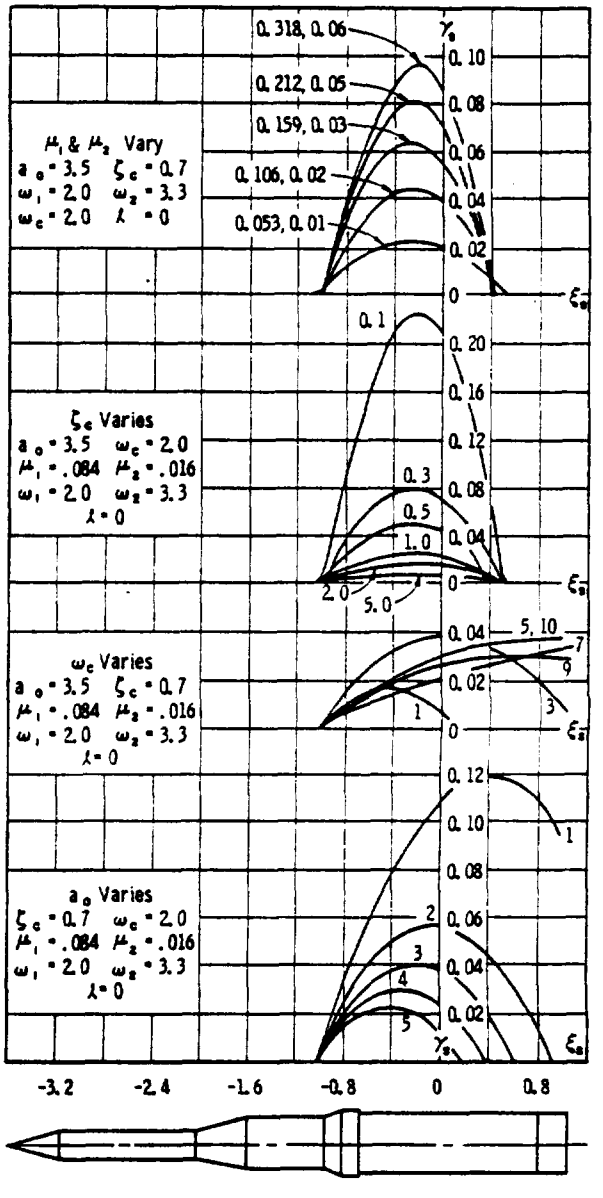

FIGURE 7.22.—Stability boundaries for sloshing in concentric tanks ($k=0.5$).

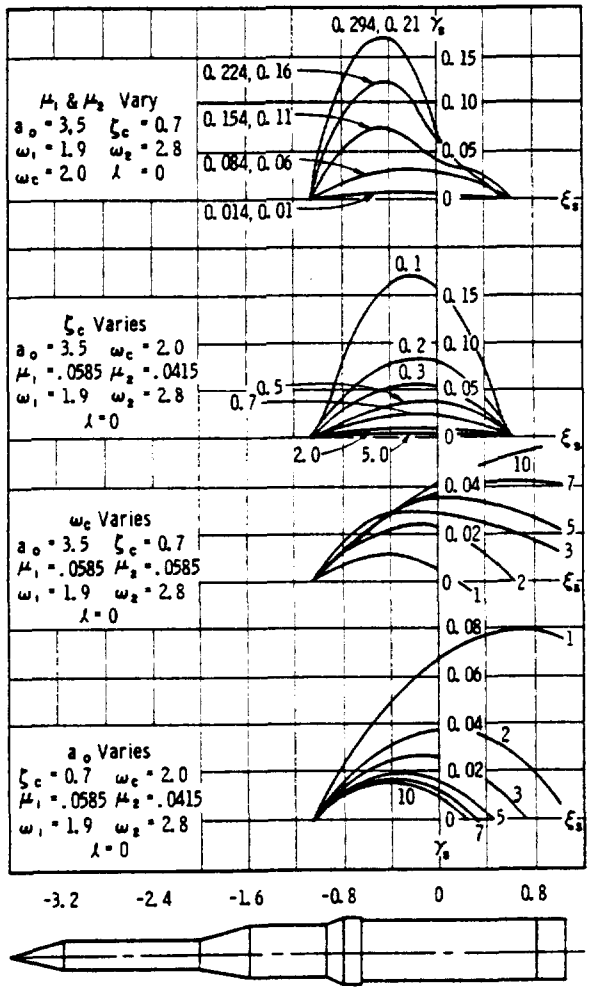

FIGURE 7.23.—Stability boundaries for sloshing in concentric tanks (k=0.7).

frequency, the stability increases. To obtain maximum cancellation effects, the sloshing masses of the center and outer container should be equal and should oscillate in antiphase. Equal sloshing masses can be obtained for a diameter ratio of about k=0.77 for which, unfortunately, the phases are not favorable. If the phases are chosen favorably, as in the case of a diameter ratio k=0.5, the sloshing masses exhibit a ratio of 1:5. This shows that no pronounced benefit can be obtained by a concentric tank arrangement. For the diameter ratios k=0.3, 0.5, and 0.7, the damping required for stability in the container is in the ratio 12:9:8.

(2) *Sector tank arrangement.*—As shown in reference 7.7, compartmentation of containers by radial walls exhibits considerably decreased sloshing masses. In the case of a quarter-tank arrangement, the first modal mass is only about a third of the value of a cylindrical container with circular cross section. But other vibration modes are still important, such as the succeeding sloshing mode of which the mass still represents 43 percent of that of the first one. This indicates that, in stability investigations, this second mode can no longer be neglected. This tank arrangement has, in addition to the reduced modal mass, the advantage that the fundamental frequency is slightly larger than that of a container of circular cross section. (See ch. 2.) Also, the total sloshing mass is distributed to various modes; thus, it is not all excited at the same frequency as in clustered tanks.

Two slosh masses are again considered in the equations of motion, representing the first and second sloshing mode of the quarter-tank arrangement; the results are very similar to the previous ones. Again, the danger zone is located between the center of instantaneous rotation and the center of mass. The increase of the control damping, ζ_c, in the subcritical region decreases the stability, while an increase in the supercritical region increases the stability region. For increasing control frequency, the danger zone is enlarged toward the base of the vehicle and requires larger damping in the tank in order to maintain stability. The influence of the simultaneous change of the sloshing frequencies shows that for sloshing frequencies below the control frequency, more baffling in an enlarged danger zone (toward the rear) is required. Increasing sloshing frequencies result in a decrease of the danger zone toward the one between the center of mass and the center of instantaneous rotation and requires less damping in the tanks to maintain stability of the vehicle. Low gain values (a_0=1) require more baffling along a larger danger zone, while an increase of the gain, a_0, reduces the danger zone and the requirement of damping in the tanks (fig. 7.24).

(3) *Tandem arrangement of two tanks.*—For a tandem-tank arrangement, the results can

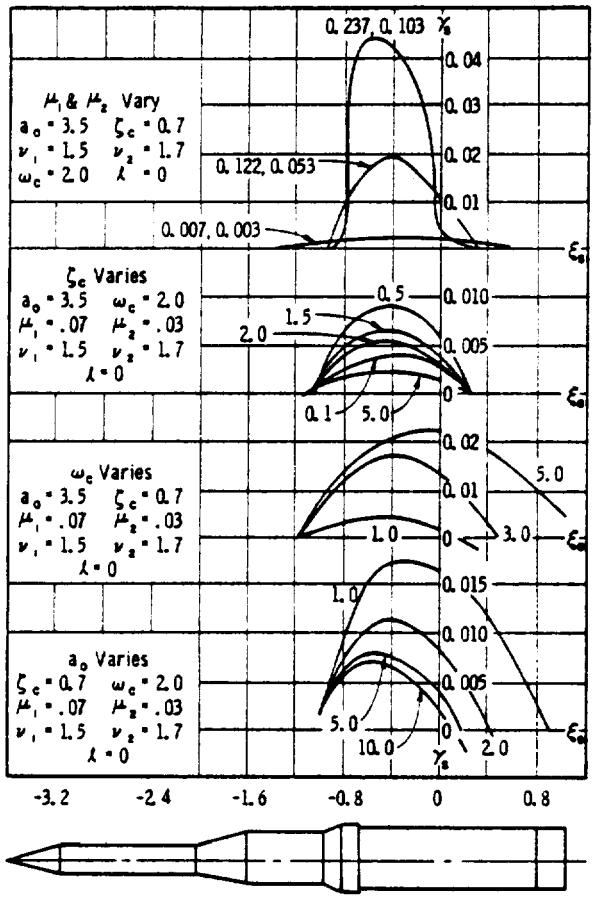

FIGURE 7.24.—Stability boundaries for sloshing in quarter-tank arrangement.

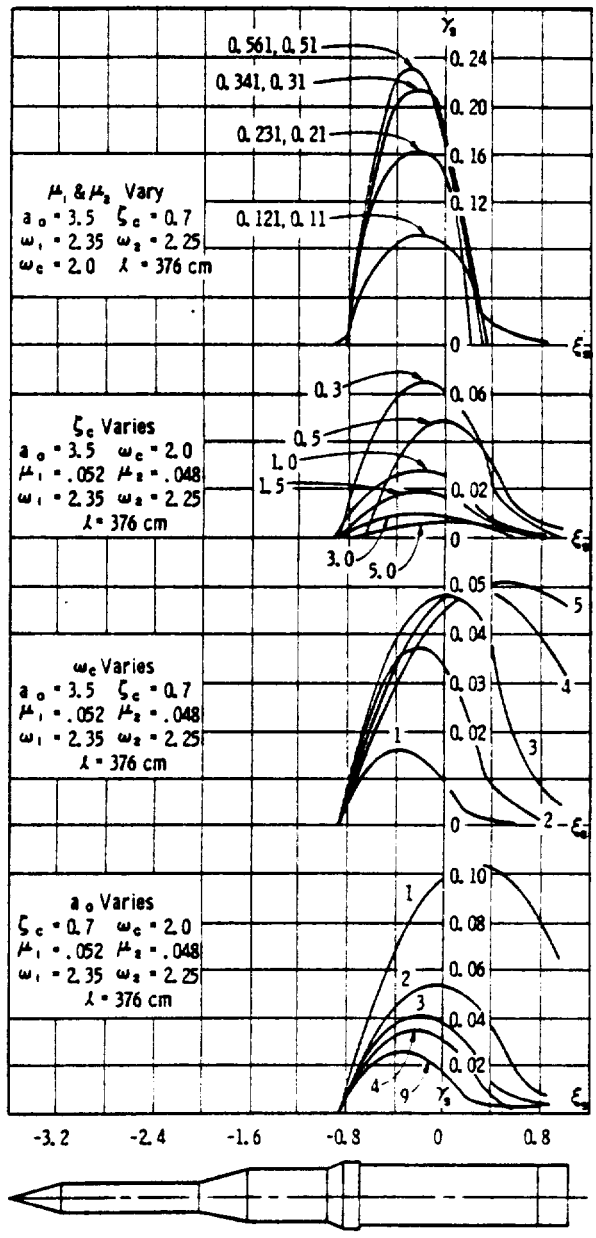

FIGURE 7.25.—Stability boundaries for sloshing in two tanks in tandem arrangement.

be seen in figure 7.25. Tank No. 1 is designated as the rear tank, and No. 2 is the forward tank. The distance between the two sloshing masses is called $l(\xi_s = l/k)$. The sloshing frequency of the liquid in these two tanks is the same. In the numerical evaluation, the diameter was taken to be approximately 100 meters (256 inches). It can be seen that for increasing sloshing mass, a loss in stability region is encountered; furthermore, the danger zone is shifted slightly toward the rear of the vehicle. Increasing control damping, ζ_c, increases the stability area. An increase of the control frequency, ω_c, results in an increased baffling requirement over an enlarged danger zone toward the aft of the space vehicle.

For sloshing frequencies below the control frequency, a large amount of damping is required in the enlarged danger zone in order to maintain stability. Increasing the sloshing frequency decreases the danger zone and the amount of damping required.

Changing the gain value, a_0, has an effect similar to that for a single tank. Small gain values require strong baffling over an enlarged danger zone. An increase in the gain value

enlarges the stability region and shifts the danger zone slightly toward the center of instantaneous rotation.

The influence of the difference, $\xi_s = l/k$, in the tank location exhibits, for increasing distance between tanks, a shifting of the danger zone aft on the vehicle, with slightly less damping requirements. This indicates that, in a vehicle in which one sloshing mass is stationary during flight and in which the other liquid mass shifts aft on the vehicle, the entire rear part of the vehicle has to be provided with appropriate damping to maintain stability (fig. 7.26).

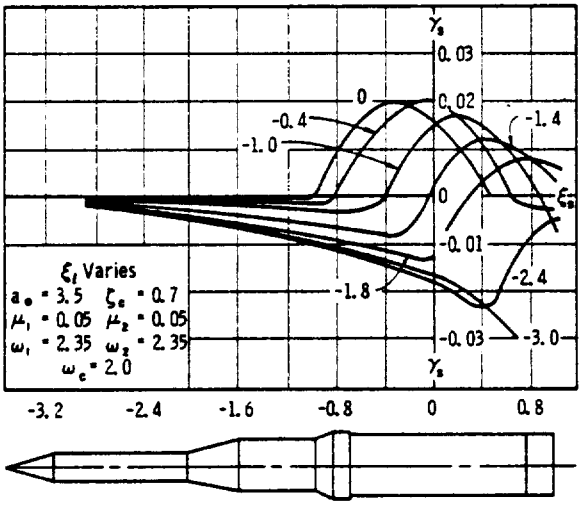

FIGURE 7.26.—Stability boundaries for rigid vehicle with simple control system and two tandem tanks (distance between tanks varying).

(4) *Tandem arrangement of three tanks.*— In almost all space vehicles, the consideration of sloshing in three propellant containers is sufficient for simplified stability boundary determinations. The liquid propellants in any remaining tanks exhibit either small sloshing masses (because of their low density or different tank geometry) or larger natural frequencies of the propellants. For this case the total determinant, equation (7.50), must be treated. The results are similar as in the tandem arrangement of two tanks. Figure 7.27 exhibits the shifting (ξ_2) of the two booster slosh masses toward the rear of the space vehicle (as it takes place during the draining of the first-

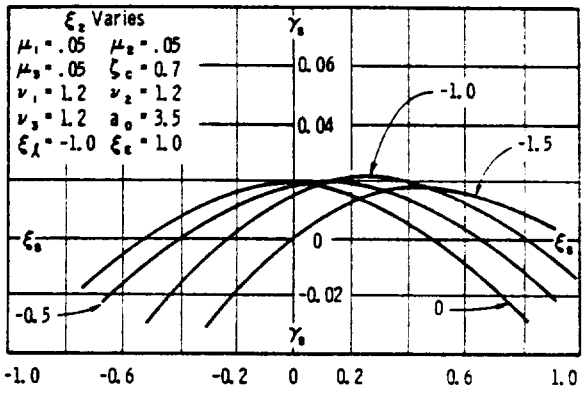

FIGURE 7.27.—Stability boundaries for sloshing in three tanks in tandem arrangement.

stage containers during first-stage flight). The danger zone shifts aft on the vehicle with increasing slosh mass difference; this again indicates that the booster must be provided with appropriate baffles to maintain stability.

For elastic vehicles, the situation changes more or less, depending on the elastic properties of the vehicle (refs. 7.20 and 7.21). This will be discussed further in chapter 9.

7.4 RESPONSE OF A VEHICLE TO ATMOSPHERIC DISTURBANCES

For satisfactory flight performance of a space vehicle, its stability is essential. This is usually obtained by proper design of the vehicle and proper choice of the control system by which the thrust vector will be controlled. In addition to the stability, the response of the system to winds must be well within the limits of the control deflections, gimbal rates, and maximum permissible structural loads on the airframe. It is therefore essential to investigate the response of the space vehicle to atmospheric disturbances. The reduction of these responses can be accomplished by proper airframe design, such that the structure can withstand the loads, and by designing the shape of the vehicle in such a fashion that aerodynamic forces and moments are minimized, as well as by a properly selected control system.

Wind buildup and gusts may require large engine deflections and engine rates, and may

induce bending vibrations and propellant sloshing. In order to study the response of a vehicle, we limit ourselves again to investigations in only one plane. This does not seem to be a significant restriction, since the interactions between pitch, yaw, and roll motions are very small for this type of vehicle. The equations of motion have been linearized and can be solved for variable coefficients by use of the Runge-Kutta method (ref. 7.22).

In the following, the numerical results are presented for a particularly large space vehicle. The complexity of the problem does not allow a detailed analytical evaluation of the equations of motion. The presentation of the results for this particular vehicle, however, should exhibit the basic idea and the valuable conclusions that can be drawn from such an investigation.

Stability

Before one can talk about the response of a vehicle, the stability of such a system has to be established. For this reason, a root locus phase study of the vehicle, with the inclusion of two bending modes and three sloshing masses (one for each of the heavy propellant tanks) is first performed. For control damping, a rate gyroscope at the engine gimbal station (a very favorable position) with a damping factor, $\zeta_G=0.7$, and a natural frequency, $f_G=16$ cps, is employed. The control frequency is considered to be 0.2 cps and the structural damping is chosen to be 1 percent. It can be shown that with a (conservative) 5-percent damping for the sloshing propellant, the vehicle is stable with respect to the propellant motion. With the bending frequencies during flight time varying from 0.8 to 1.2 cps in the first bending mode and from 1.9 to 2.5 cps in the second bending mode, the system was found to be stable. In this particular case, the second of the bending modes exhibited the smallest stability.

Wind Response

After the stability of all generalized coordinates has been established, the response of the space vehicle resulting from some atmospheric disturbance can be investigated. In order to determine the influence of the vehicle flexibility and propellant sloshing in the tanks, four different cases are studied:

(1) Rigid vehicle with no sloshing in the propellant tanks.

(2) Rigid vehicle with propellant sloshing in the three heavy tanks (No. 1: LOX tank of the booster stage; No. 2: Fuel tank of the booster stage; No. 3: LOX tank of the second stage).

(3) Elastic vehicle with no sloshing in the propellant tanks.

(4) Elastic vehicle with propellant sloshing in the three heavy tanks.

The input used is a 95-percent probability wind building up in about 11½ seconds to a value of 75 m/sec. To this wind, starting at 58.5-seconds flight time, a 9-m/sec gust is added which starts at 70-seconds flight time, remains at 84 m/sec for about 1 second (an altitude band of about 250 meters) and then drops down to 75 m/sec (fig. 7.28). This occurs at a flight time of 70 seconds where the product of angle of attack and dynamic pressure assumes its maximum value. At that flight time, the sloshing frequencies in the tanks were:

Fundamental sloshing frequency in tank 1: $f_{1_1}=0.44$ cps
Fundamental sloshing frequency in tank 2: $f_{2_1}=0.445$ cps
Fundamental sloshing frequency in tank 3: $f_{3_1}=0.45$ cps

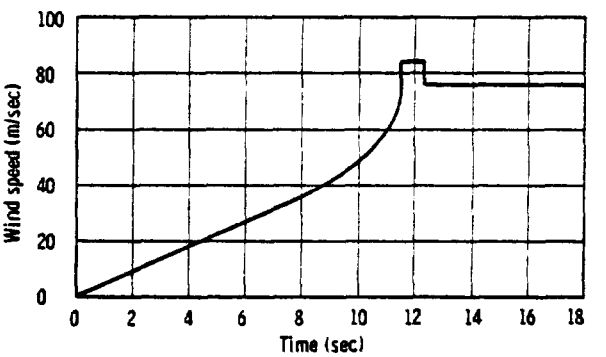

FIGURE 7.28.—Wind buildup and gust.

The bending frequencies were:

First bending: $f_{1B}=1.15$ cps
Second bending: $f_{2B}=1.92$ cps

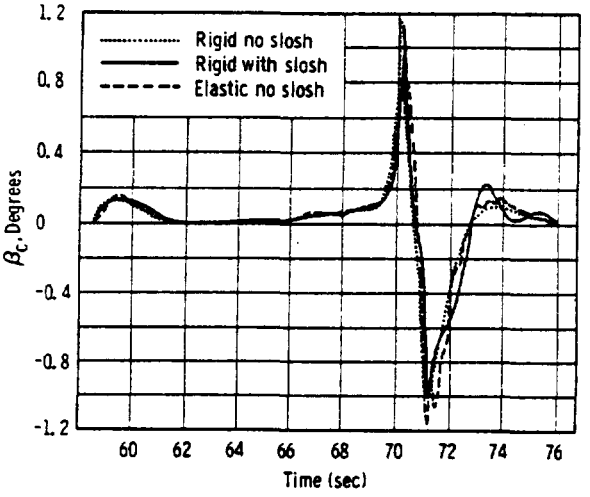

FIGURE 7.29.—Response analysis: Engine command signal.

In figures 7.29 through 7.40, the response of each of the various generalized coordinates is compared to that of the rigid vehicle without and with liquid sloshing and the elastic vehicle without sloshing. Here, the influence of sloshing in a rigid vehicle as well as the elastic influence can be obtained. Figure 7.29 shows the engine deflection β_c, reaching an angle of about 1.2° after the gust hits the vehicle. The value for a rigid vehicle without sloshing exhibits a slightly larger magnitude. After the gust has been applied, the sloshing liquid requires a little more than 0.1° engine deflection; the engine follows the propellant motion with a frequency of about 0.45 cps. This oscillation exhibits a damping value of about 6 percent. The elastic vehicle shows a slightly smaller maximum peak value; it requires, however, a little larger engine deflection in the transient than does the rigid vehicle. The oscillation of the engine deflection is at a frequency of about 2 cps and has an amplitude of about 0.015°, showing that the less stable second mode has been excited.

A similar behavior can be detected in figure 7.30 for the rate of the engine deflection, with the exception that $\dot{\beta}_c$ reaches its stop of 5°/sec. The three cases show no appreciable difference in the attitude angle (fig. 7.31). It reaches its peak of about 4° shortly after the gust has disappeared. The elasticity of the vehicle increases the angle slightly by a value of about

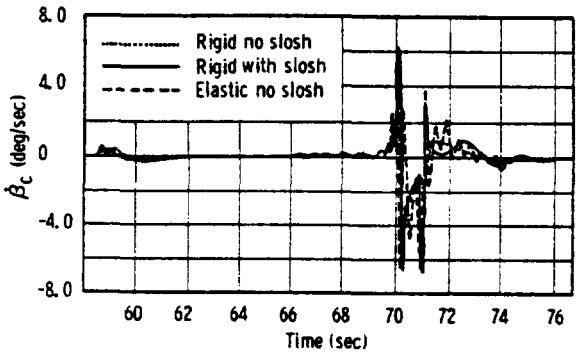

FIGURE 7.30.—Response analysis: Engine command rate.

0.1°. Figure 7.32 shows the result for $\ddot{\phi}$ in deg/sec^2. The angle of attack, α, is exhibited in figure 7.33 and presents a maximum value of about 10° at the time the gust is applied. Sloshing and elasticity of the vehicle result only in very small differences compared with the rigid vehicle. The same is true for the translational displacement, y, of the vehicle (fig. 7.34). The translational acceleration of the vehicle exhibits the fact that translational sloshing results in a larger disturbance than does sloshing resulting from pitching (fig. 7.35). The vehicle performs translational oscillations with a frequency of 0.45 cps as a result of the propellant oscillations in the tanks. Elastic oscillations have only a minor effect. After the gust has hit the rigid vehicle, the propellant in the first tank (LOX tank of the booster stage) reaches a maximum amplitude of 21 centimeters and performs a damped oscillation

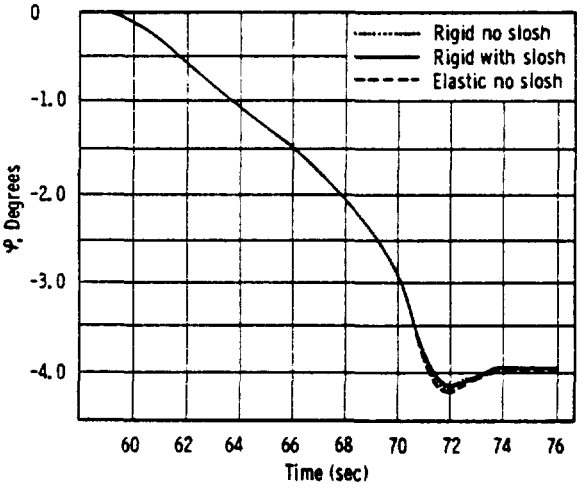

FIGURE 7.31.—Vehicle rotation.

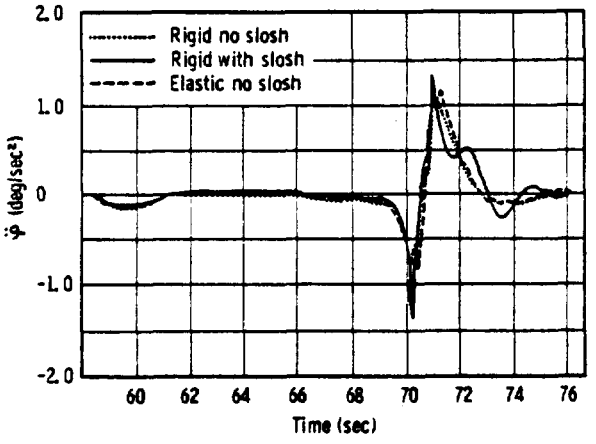

FIGURE 7.32.—Vehicle angular acceleration.

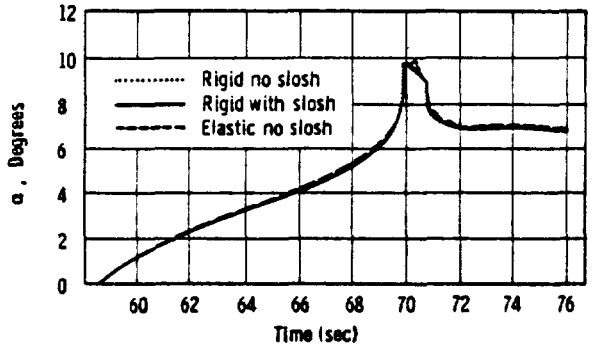

FIGURE 7.33.—Angle of attack.

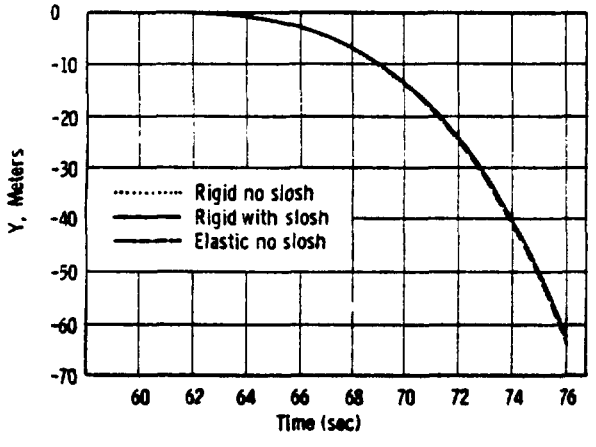

FIGURE 7.34.—Vehicle translation.

with about 5 percent damping (fig. 7.36). The propellant in the second tank (fuel tank of the booster stage) reaches a maximum of 13 centimeters (fig. 7.37). The amplitude of the pro-

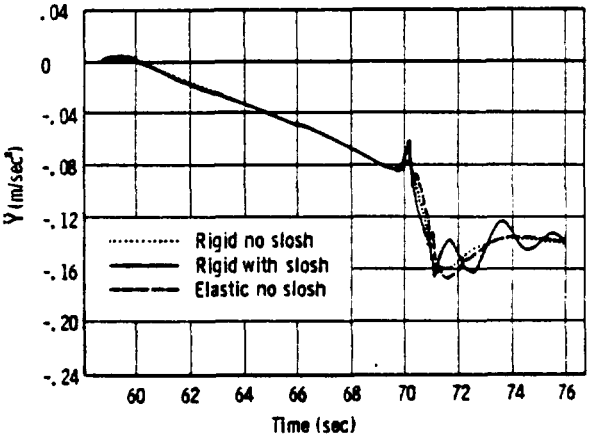

FIGURE 7.35.—Vehicle translatory acceleration.

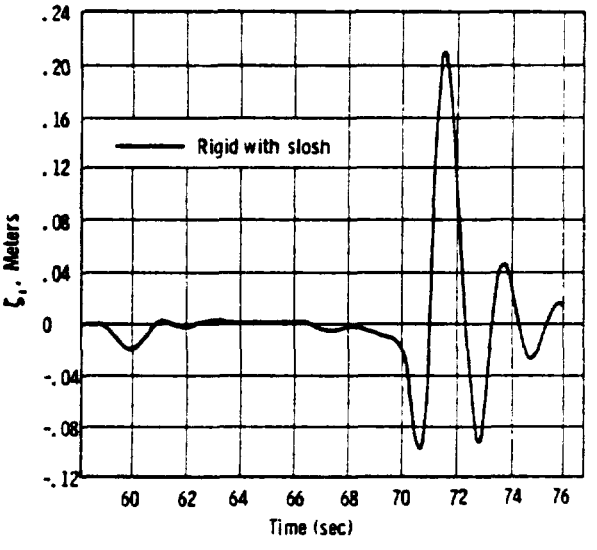

FIGURE 7.36.—First-slosh amplitude.

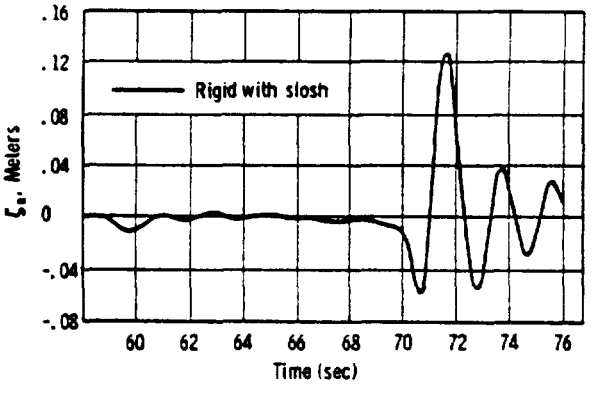

FIGURE 7.37.—Second-slosh amplitude.

pellant in the third tank (LOX tank of the S–II stage) is 4 centimeters (fig. 7.38), and remains constant for a larger time period. For the elastic vehicle without propellant sloshing, the first bending mode has a maximum displacement of the generalized coordinate, η_1, of 1.7 centimeters right after the gust has hit the vehicle (fig. 7.39). The second mode exhibits only 4½ millimeters, but shows sustained vibrations of one-tenth of a millimeter in the transient, indicating that this has a frequency content to which the second bending mode is susceptible (fig. 7.40).

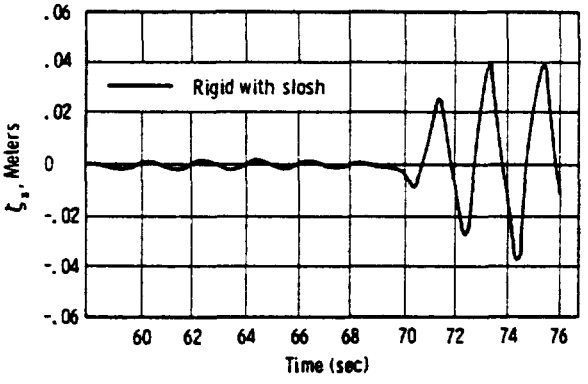

FIGURE 7.38.—Third-slosh amplitude.

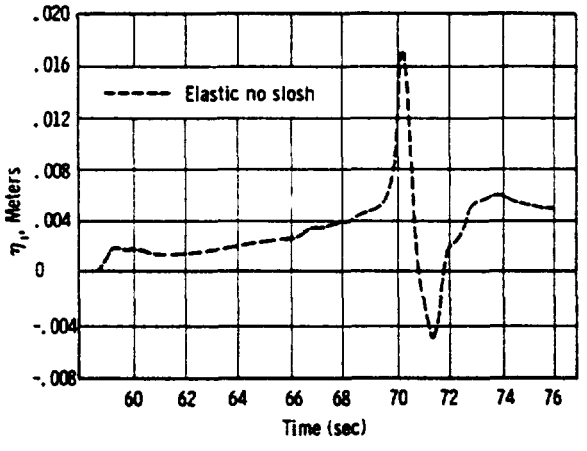

FIGURE 7.39.—First bending deflection.

Figures 7.41 through 7.52 compare the response of the elastic vehicle with propellant sloshing in its tanks with that of the elastic vehicle without sloshing and with that of the rigid vehicle with sloshing. In figure 7.41, it can be seen that the engine deflection at about

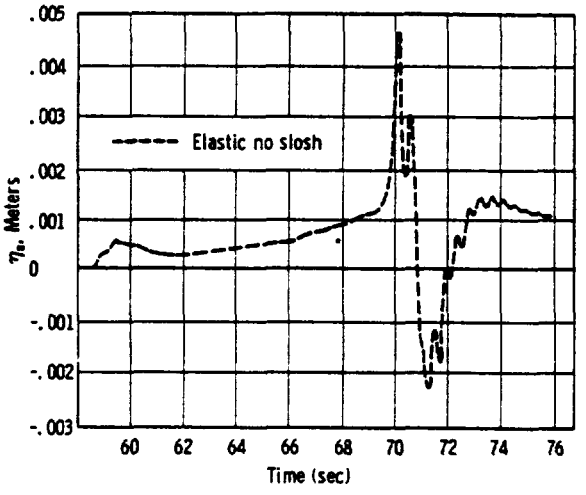

FIGURE 7.40.—Second bending deflection.

the time the gust is applied is about 1.2° and slightly less for the elastic vehicle. Then the engine performs a damped oscillation which is always forced to react to the sloshing of the propellant and exhibits a slightly larger value for the elastic vehicle. If propellant sloshing is suppressed, the engine performs small oscillations at the frequency of the second bending mode. As can be seen in figure 7.42, the stop of 5°/sec for $\dot{\beta}_c$ has again been reached. There is not much difference indicated in the attitude angle, $\phi(\approx 4°)$, as shown in figure 7.43. Figure 7.44 shows $\ddot{\phi}$. The angle of attack, α, reaches a maximum of 10°, but the difference between the rigid and elastic vehicle is only minor

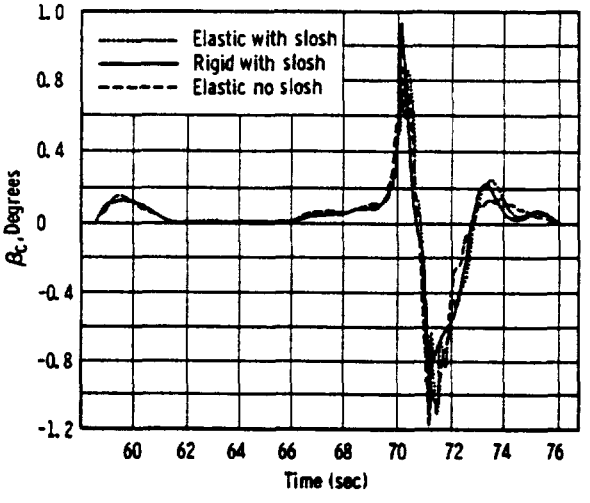

FIGURE 7.41.—Engine command signal.

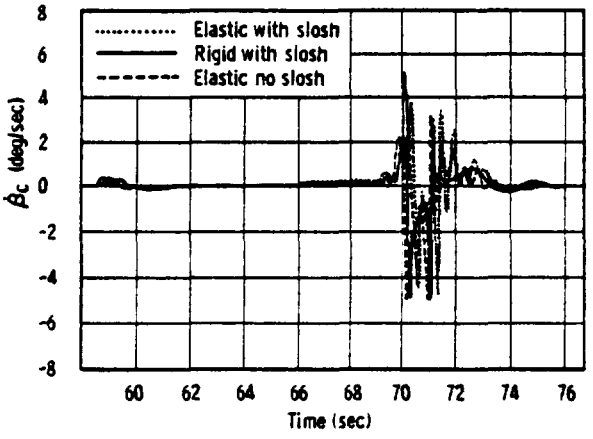

FIGURE 7.42.—Engine command rate.

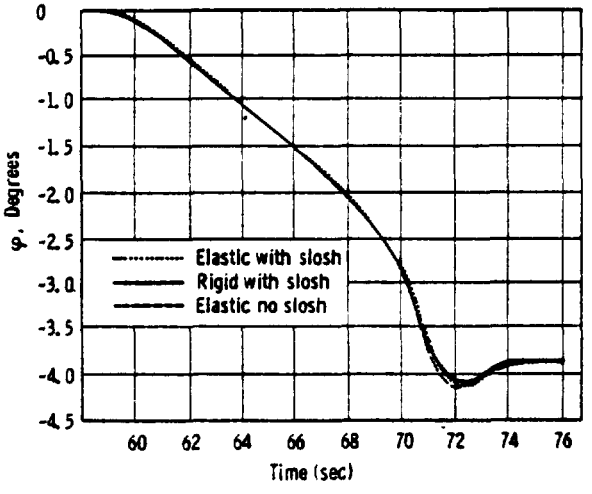

FIGURE 7.43.—Vehicle rotation.

(fig. 7.45). The translation of the vehicle is given in figure 7.46 and exhibits only very slight differences between the various cases. The translational acceleration, however, indicates immediately the effect of propellant sloshing. The maximum acceleration is 17 cm/sec^2 (fig. 7.47). The propellant exhibits a maximum amplitude of 21 centimeters in container No. 1. Elastic and rigid vehicles show nearly the same value, except that in the elastic case the peaks come at a slightly later flight time (fig. 7.48). In the second tank (fig. 7.49), the maximum is 13 centimeters for a rigid vehicle and about 1½ centimeters higher for the elastic vehicle. This is because the bending mode at this tank location exhibits a larger

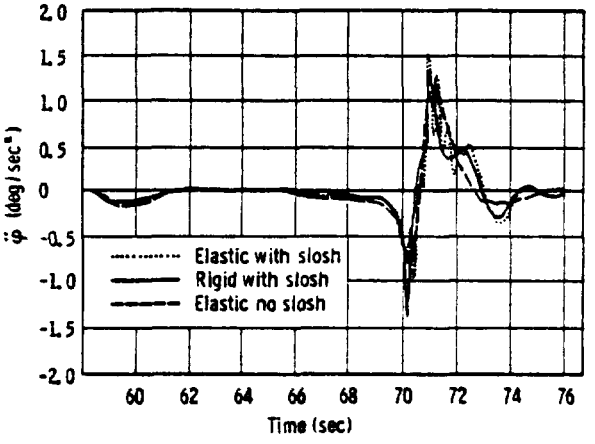

FIGURE 7.44.—Vehicle angular acceleration.

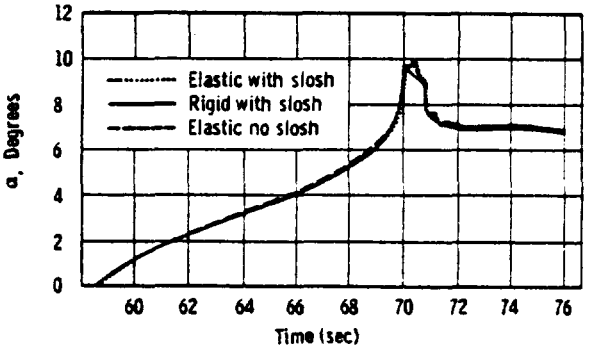

FIGURE 7.45.—Angle of attack.

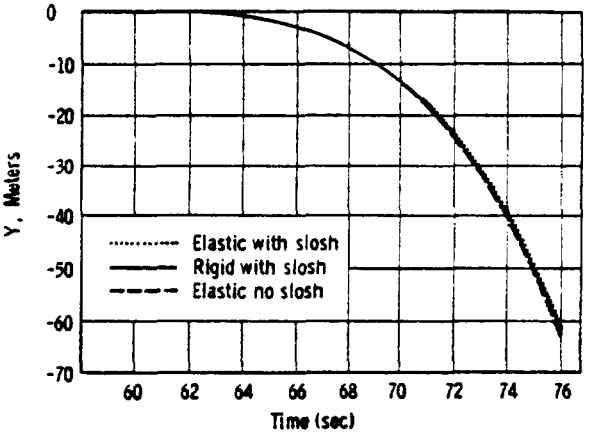

FIGURE 7.46.—Vehicle translation.

deflection. This effect is increased for the third tank, which is even closer to the antinode of the bending mode and is also located in the danger zone between center of mass and the center of instantaneous rotation where more baffling is

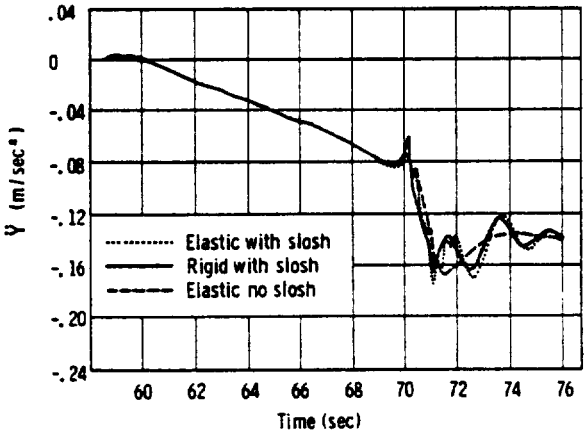

FIGURE 7.47.—Vehicle translatory acceleration.

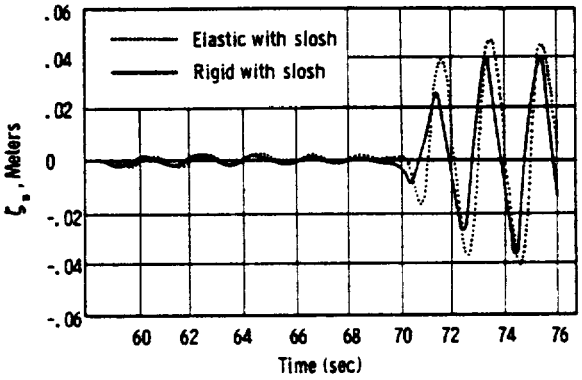

FIGURE 7.50.—Third-slosh amplitude.

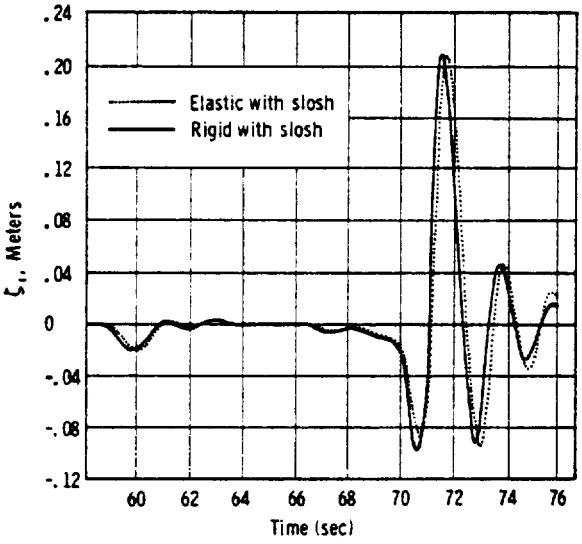

FIGURE 7.48.—First-slosh amplitude.

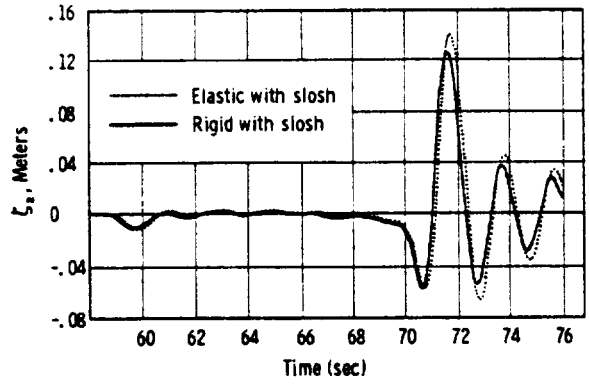

FIGURE 7.49.—Second-slosh amplitude.

required. In figure 7.50, the maximum sloshing amplitude of a rigid vehicle is 4 centimeters, while for an elastic vehicle the amplitude reaches 5 centimeters. The propellant motion exhibits very little damping. The first bending mode is represented in figure 7.51, and reaches its peak of 1.7 centimeters right after the gust has hit the vehicle (the sloshing influences the transient). The second bending mode, shown in figure 7.52, has a maximum value of 4.5 mm and exhibits larger but (because of the low frequency sloshing) smoother values in the transient. In both bending modes, the presence of sloshing propellant influences the decay of the bending motion of the space vehicle.

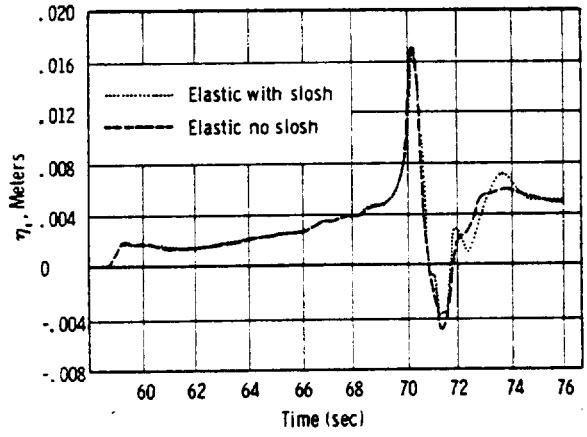

FIGURE 7.51.—First bending deflection.

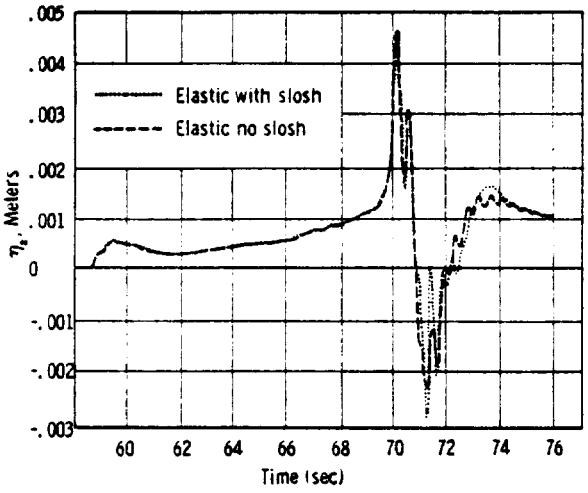

FIGURE 7.52.—Second bending deflection.

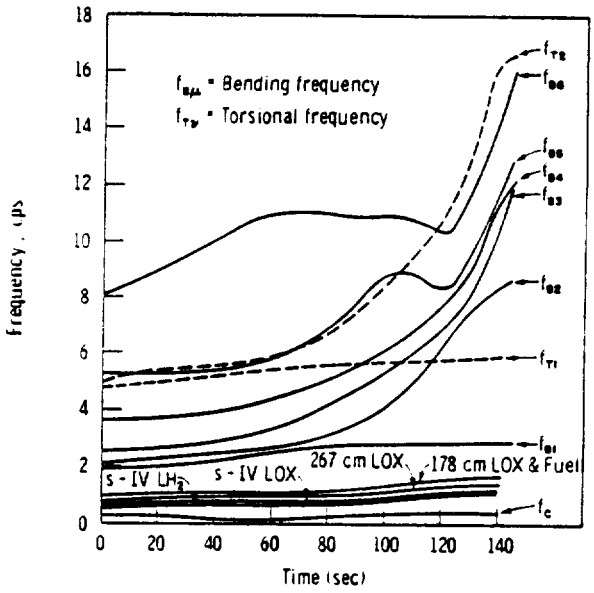

FIGURE 7.53.—Frequency spectrum versus flight time.

7.5 EXAMPLE

The following is a simple example which employs the previous results. A Saturn I-type vehicle for which half of the thrust ($\epsilon=\frac{1}{2}$) is available for control purposes is used. The Saturn I booster is powered by a cluster of eight engines, each of which will produce 188000 pounds of thrust to give a total of 1.5 million pounds. The booster is about 6.55 meters in diameter and 25 meters in length. The total length of the vehicle is about 51.8 meters. The eight engines are arranged in two square patterns, of which the inner ones are rigidly attached, while the outer engines are mounted on gimbals which permit them to be turned through angles of about 10° to provide control of the vehicle during first-stage powered flight. Nine separate tanks feed the eight engines. Clustered in a circle about a center tank of 267 centimeters in diameter are eight small tanks of 178 centimeters each in diameter. The center tank (noted as tank No. 1) and four outer containers (noted as tank No. 2) contain liquid oxygen, while the remaining four outer containers (noted as No. 3) contain fuel (RP-1). The S-IV, which is the second stage, is powered by six 15,000-pound-thrust liquid hydrogen/liquid oxygen engines. This stage has a diameter of about 5.5 meters and is about 12.2 meters long. A look at the frequency spectrum versus flight time (fig. 7.53) reveals that the control feedback stability problem is a quite involved one. The purpose of such an exercise is to decide early enough in the planning stage as to how the vehicle should be efficiently designed.

The sloshing frequencies range from about 0.5 cps to 1.5 cps. At 140-seconds flight time, the four inboard engines are shut down, which decreases the longitudinal accelerations and is exhibited in the graph by the abrupt drop of the propellant frequencies. The smaller natural frequencies in the 267-centimeter-diameter containers compared to the 178-centimeter container are the result of its larger tank diameter. The same effect, and the smaller liquid height, contributes to the small sloshing frequency in the S-IV LOX tank. The control frequency is in the neighborhood of 0.2–0.3 cps, while the first lateral bending frequency ranges from about 2 to 2.4 cps during booster flight. The location of the mass center and the center of instantaneous rotation of the vehicle, as well as the location of the sloshing masses, for booster flight is shown in figure 7.54. Since the sloshing propellant masses are of great importance upon the dynamics of the vehicle, their magnitude is presented in figure 7.55 as the ratio of the mass of the sloshing propellant in a container

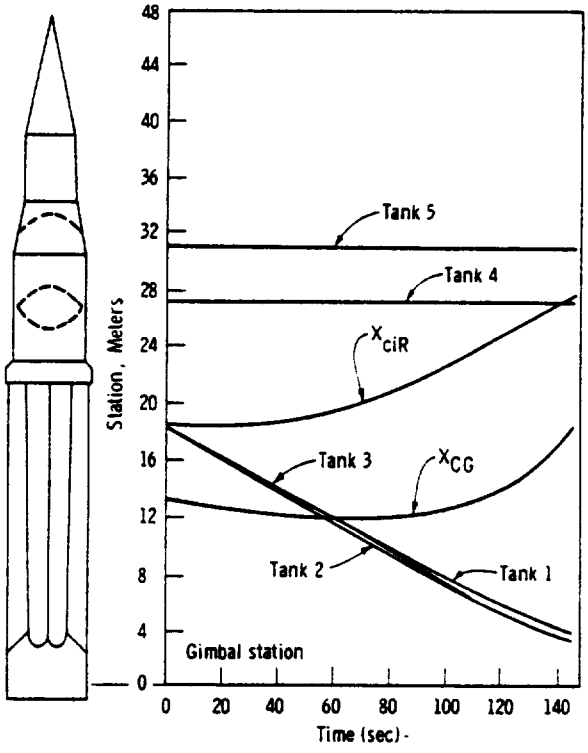

FIGURE 7.54.—Slosh mass location versus booster flight time.

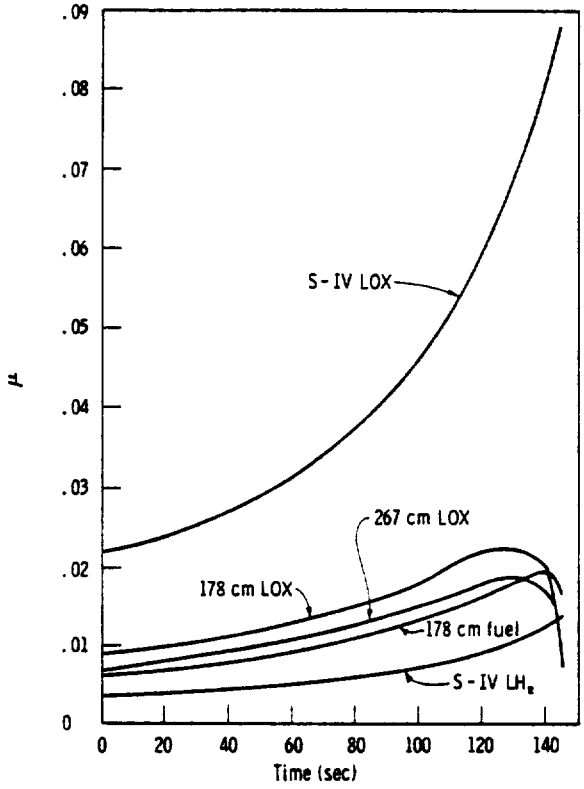

FIGURE 7.55.—Slosh mass ratio for SA-I booster flight.

to the total vehicle mass, versus booster flight time. Immediately, it can be seen that the LOX tank of the S–IV stage which exhibits (because of the mass change of the vehicle with booster flight time) large values will have a very pronounced effect upon the stability of the vehicle.

In the following, we shall apply the results of this chapter. The frequency ratios, $\nu_s = \omega_s/\omega_c$, are always larger than unity, thus indicating a favorable situation. The gain value is $a_0=1.5$ and changes, at a flight time of 110 seconds, to the magnitude $a_0=1$. If only one mass were sloshing, say that of the S–IV LOX container, the conclusions we could draw at a flight time of 70 seconds, where $\mu=0.03$, $\zeta_c=0.7$, $\nu_s\approx 3$, and $\xi_s\approx -1.2$, from figure 7.13 would be the following: for this flight time no damping would be needed in this container since it is located outside the danger zone, i.e., outside the zone between center of mass and center of instantaneous rotation; at a flight time of 140 seconds, where $\mu=0.09$, $\nu_s=4$, and $\xi_s\approx -0.9$, a little damping in the amount of about $\gamma_s\approx 0.005$ would be needed to maintain stability.

Combining all sloshing masses of the booster in one mass and considering the effect of the S–IV stage sloshing masses as negligible yields the following: first of all, at a flight time of 70 seconds, the combined slosh mass ratio μ would be of the magnitude of about $\mu=0.09$; the frequency ratio, ν_s, is about $\nu_s\approx 3$, and the location $\xi_s\approx 0$. For this particular case, a damping of about 1 percent should be provided. At a flight time of 140 seconds, $\mu=0.18$, $\nu_s=4$, and $\xi_s=0.8$, no damping is needed since the sloshing mass is located outside of the danger zone. From this simple consideration, one can conclude that a stationary baffle arrangement in the upper part of the booster tanks is sufficient to maintain flight stability during the boost phase.

To obtain, however, a more realistic requirement, we have to look at the sloshing in several containers. Considering the S–IV LOX slosh-

ing mass together with the combined booster sloshing mass, one can use the results presented in figures 7.25 and 7.26. At 70-seconds flight time, the sloshing masses are given by $\mu_1=0.09$ and $\mu_2=0.03$, while $\nu_1=\nu_2\approx 3$. The distance l of the combined booster sloshing mass, μ_1, to the fixed sloshing mass, μ_2, of the second stage is $l\approx -16.25$ meters; that is, $\xi_l\approx -1.3$. The value $\xi_s\approx 0$, and we conclude that a damping of $\gamma_s\approx 0.013$ is needed to have a stable flight condition. At a flight time of 140 seconds, $\mu_1=0.18$, $\mu_2=0.09$, $\nu_1\approx\nu_2\approx 4$, $\xi_s=0.8$, and $\xi_l\approx -1.8$, and a damping of about 1 percent is needed. It furthermore can be seen that damping is needed in the lower part of the booster containers. Since the fundamental bending frequency is close to the sloshing frequencies, the effects of vehicle elasticity (ch. 9) must also be considered. Furthermore, some wind response studies will show the adequacy of the baffles. (See sec. 7.4.)

The actual feedback analysis of the flexible vehicle with all its slosh masses included indicated that with smooth container walls a slight instability occurred in the 178-centimeter containers between 40- and 60-seconds flight time, and in the 267-centimeter-diameter container an instability occurs between 60- and 90-seconds flight time (ref. 7.23). By employing proper baffles, these instabilities could be removed. The same procedure can now be performed for the second-stage flight, but has been omitted here for reasons of limited space.

REFERENCES

7.1. Bauer, H. F.; and Rheinfurth, M. H.: Flutter and Stability Analysis. Army Ballistic Missile Agency, Redstone Arsenal, Ala., DA-TM-4-60, 1960.

7.2. Rheinfurth, M. H.: Control Feedback Stability Analysis. Army Ballistic Missile Agency, Redstone Arsenal, Ala., DA-TR-2-60, 1960.

7.3. Thorp, F. A.; and Hutchinson, R. C.: The Dynamics of Rocket-Powered Vehicles. Massachusetts Institute of Technology, Rept. R-206, Feb. 1959.

7.4. Lukens, D. R.; Schmitt, A. F.; and Broucek, G. T.: Approximate Transfer Function for Flexible - Booster - and - Auto - Pilot Analysis. WADD-TR-61-93, 1961.

7.5. Barton, M.: Generalized Missile Dynamics Analysis. Ramo-Wooldridge Corp., 1958.

7.6. Heist, E. K.: Equations of Motion of Missile With Sloshing. Guided Missile Research Division, Ramo-Wooldridge Corp. Rept. No. GM-TM-146, 1956.

7.7. Bauer, H. F.: Fluid Oscillations in the Container of a Space Vehicle and Their Influence Upon Stability. NASA-TR R-187, 1964.

7.8. Bauer, H. F.: Dynamics of Liquid Propellant Vehicles. Proceedings of the ONR/AIA Symposium on Structures and Dynamics of High Speed Flight, ONR/AIA Symposium, 1961.

7.9. Bauer, H. F.: The Effects of Interaction of Structure, Control and Propellant Sloshing Upon the Stability of Large Space Vehicles. Marshall Space Flight Center, NASA, MTP-AERO-61-83, 1961.

7.10. Zurmühl, R.: Praktische Mathematik für Ingenieure und Physiker. Springer-Verlag, Berlin, 1953.

7.11. Brodetsky, S.; and Smeal, G.: On Graeffe's Method for Complex Roots of Algebraic Equations. Proc. Cambridge Phil. Soc., vol. 22, 1924, pp. 83–87.

7.12. Routh, E. J.: A Treatise on the Stability of a Given Motion. Macmillan, London, 1877, pp. 74–81.

7.13. Hurwitz, A.: Uber die Bedingungen unter welchen eine Gleichung nur Wurseln mit negative reellen Theilen besitzt. Mathematische Annalen, vol. 46, 1895, pp. 273–284.

7.14. Nyquist, H.: Regeneration Theory. Bell System Technical Journal, vol. 11, 1932, 126–147.

7.15. Rheinfurth, M. H.: The Influence of Control Sensors on the Stability of Space Vehicles. Marshall Space Flight Center, NASA, MTP-61-65, 1961.

7.16. Bauer, H. F.: The Effects of Propellant Sloshing on the Stability of an Accelerometer Controlled Rigid Space Vehicle. NASA TN D-1831, 1963.

7.17. Bauer, H. F.: Stability Boundaries of Liquid Propelled Space Vehicles With Sloshing. AIAA J., vol. 1, no. 7, 1963.

7.18. Heinrich, K.; and Kaufman, F. H.: Sloshing Stability Criteria for Vehicles With One Free Fluid. Ramo-Wooldridge Memo GM-45.3-45, 1956.

7.19. Fuller, A. T.: Stability Criteria for Linear Systems and Reliability Criteria for RC Networks. Proc. Cambridge Phil. Soc., vol. 53, 1957, pp. 878–896.

7.20. Geissler, E. D.: Problems in Attitude Stabilization of Large Guided Missiles. Aero-Space Engineering, Oct. 1960, pp. 24–29.

7.21. Bauer, H. F.: Parametric Study of the Influence of Propellant Sloshing on the Stability of Space Crafts. J. Aerospace Sci., Oct. 1961, pp. 819–820.
7.22. Bauer, H. F.: Wind Response of the Saturn LOR Vehicle. Marshall Space Flight Center, NASA, MTP-AERO-63-19, 1963.
7.23. Hays, P. J., and Sumrall, J. P.: Stability Analysis of Saturn SA-5 With Live S-IV Stage. NASA TM-X-53017, 1964.

PRINCIPAL NOTATIONS

a_0 = gain factor of attitude channel
a_1 = coefficient of control damping
A_t = output signal of accelerometer
A_s = shear area of airframe cross section
c_a = damping coefficient of accelerometer
c_G = damping coefficient of rate gyroscope
$c_{n\lambda}$ = damping coefficient of nth sloshing mode in λth propellant container
D = dissipation function
D_p = dissipation function of propellant
D_s = dissipation function of vehicle structure
EI = flexural stiffness of airframe
$F = F_1 + F_2$ = thrust
F_1 = stationary thrust
F_2 = gimbal thrust
$g = \frac{F}{m}$ = longitudinal vehicle acceleration
g_ν = structural damping factor of the νth bending mode
g_2 = gain factor of accelerometer channel
G = shear modulus
H_ν = Hurwitz determinant
I = mass moment of inertia of total vehicle about mass center of vehicle
I_G = moment of inertia of rate gyroscope about its output axis
$I_{0\lambda}$ = moment of inertia of nonsloshing liquid mass in λth propellant container (about its center of mass)
I_R = moment of inertia of rotor of rate gyroscope about spin axis
I'_s = moment of inertia of structure per unit length
k = radius of gyration of vehicle about its mass center
k_a = spring constant of accelerometer
k_E = spring constant of swivel compliance
$k_{n\lambda}$ = spring constant of nth mode of slosh model in λth tank
K_G = restoring moment of rate gyroscope per unit angle
m = mass of vehicle
m_a = mass of accelerometer
$m_{n\lambda}(m_s)$ = mass of nth sloshing mode in λth tank
$m_{0\lambda}$ = mass of nonsloshing liquid in λth tank
m'_s = mass of structure per unit length
$M_{B\nu}$ = generalized mass of νth bending mode
M_R = gyroscopic reaction torque of rate gyroscope
M_ν = bending moment of νth bending mode
$_1p\ p_2$ = phase-lag coefficients of control system
q_i = generalized coordinates
Q_i = generalized forces
Q_ν = shear force of νth bending mode
$s = \sigma + i\omega$ = complex frequency
t = time
T = kinetic energy
T_p = kinetic energy of propellant
T_s = kinetic energy of structure
v = cross-velocity
V = potential energy of vehicle
V_p = potential energy of propellant
V_{sE} = potential energy of elastic deformation of structure
V_{sg} = potential energy of raising center of mass in equivalent gravitational field
V_ν = potential energy of bending vibration
x = abscissa, distance from mass center
x_a = coordinate of accelerometer
$|x_{cIR}|$ = distance of center of instantaneous rotation to mass center of vehicle

x_B = coordinate of swivel point

x_G = coordinate of gyroscope

$x_{n\lambda}(x_s)$ = coordinate of sloshing mass of nth mode in λth tank

$x_{0\lambda}$ = coordinate of nonsloshing mass in λth tank

x_R = coordinate of rate gyroscope

y = lateral translation of rigid vehicle

y_a = displacement of accelerometer mass relative to vehicle

$y_{n\lambda}$ = displacement of nth sloshing mass in λth container relative to vehicle

Y_ν = normalized bending deflection curve of νth bending mode

$\alpha = \frac{x_a}{|x_{c1R}|}$ = location parameter of accelerometer

β = engine deflection angle against vehicle center axis

β_c = control deflection

γ_s = slosh damping factor

$\epsilon = \frac{F_2}{F}$ = ratio of thrust available for control purpose to total thrust of vehicle

ϵ_a = abbreviation for accelerometer defined on page 242

ϵ'_a = abbreviation for accelerometer defined on page 242

ϵ'_G = abbreviation for gyroscope defined on page 239

ϵ'_R = abbreviation for rate gyroscope defined on page 239

ζ_a = damping factor of accelerometer

ζ_c = damping factor of control system

ζ_G = damping factor of rate gyroscope

$\zeta_{n\lambda}$ = damping factor of nth sloshing mode in λth tank

η_ν = generalized coordinate of νth bending mode

θ_i = indicated angular velocity of airframe at the location of the rate gyroscope

$\left.\begin{matrix}\lambda = \epsilon g g_2 \\ \lambda = g g_2\end{matrix}\right\}$ = "gain parameter" of accelerometer

$\mu_{n\lambda} = \frac{m_{n\lambda}}{m}$ = slosh mass ratio of nth sloshing mode in λth container to total vehicle mass

$\nu_a = \omega_a/\omega_c$ = frequency ratio of accelerometer to control frequency

$\nu_s = \omega_s/\omega_c$ = frequency ratio of propellant to control frequency

$\xi_a = \frac{x_a}{k}$

$\xi_d = \frac{x_d}{k}$

$\xi_E = \frac{x_E}{k}$

$\xi_l = \frac{x_l}{k}$

$\xi_s = \frac{x_s}{k}$

ϕ = rotation angle of rigid vehicle relative to space

ϕ_i = output signal of attitude gyroscope

$\dot{\phi}_R$ = angular velocity of airframe at the location of the rate gyroscope

ω_a = natural circular frequency of accelerometer

ω_c = natural circular control frequency

ω_G = natural circular frequency of rate gyroscope

$\omega_{n\lambda}(\omega_s)$ = natural circular frequency of nth propellant mode in λth container

ω_R = angular velocity of rotor in rate gyroscope

ω_ν = natural circular frequency of νth bending mode